

RESEARCH

Open Access



From pilot knowledge via integrated reservoir characterization to utilization perspectives of deep geothermal reservoirs: the 3D model of Groß Schönebeck (North German Basin)

Ben Norden^{1*} , Klaus Bauer¹ and Charlotte M. Krawczyk^{1,2}

*Correspondence:
ben.norden@gfz-potsdam.de

¹ GFZ German Research Centre for Geosciences, Telegrafenberg, 14473 Potsdam, Germany

² TU Berlin, Institute for Applied Geosciences, Ernst-Reuter-Platz 1, 10587 Berlin, Germany

Abstract

The Groß Schönebeck site in the North German Basin serves as research platform to study the geothermal potential of deeply buried Permian reservoir rocks and the technical feasibility of heat extraction. The structural setting of the site was investigated in more detail by a newly acquired 3D-seismic survey to improve the former conceptual model that was based on several old 2D seismic lines. The new data allow a revision of the geological interpretation, enabling the setup of a new reservoir model and providing base information for a possible further site development of Permo-Carboniferous targets. The 3D seismic allows for the first time a consistent geological interpretation and model parameterization of the well-studied geothermal site. Main reflector horizons and the corresponding stratigraphic units were mapped and the structural pattern of the subsurface presented in the 8 km × 8 km × 4 km large seismic volume. Attribute analysis revealed some fracture and fault patterns in the upper Zechstein and post-Permian units, while formerly hypothesized large offset faults are not present in the Rotliegend reservoir. However, a well-established graben-like structure at the top of the Zechstein succession is most likely related to broken anhydritic brittle intra-salt layers of some meter of thickness. Most reflectors above the salt show a rather undisturbed pattern. The main reservoir sandstone of the Dethlingen Formation (Rotliegend) was mapped and characterized. The base of the underlying Permo-Carboniferous volcanic rock sequence and hence its thickness could not be depicted reliably from the geophysical data. Based on the seismic data and the available reconnaissance drilling, logging, and laboratory data of the Groß Schönebeck research site, the thickness and distribution of the sedimentary Rotliegend (with emphasis of the sandy reservoir section) and of the volcanic rock sequence was modelled and stochastically parameterized with petrophysical properties guided by seismic facies pattern correlation, providing a more realistic reservoir description. Properties include total and effective porosity, permeability, bulk density, thermal conductivity, thermal diffusivity, and specific heat capacity. The data and interpretation constitute the basis for a better understanding of the thermo and hydromechanical processes at the site and for future measures. Further

site development could include a deepening of one well to provide evidence on the volcanic rock sequence and consider deviated wells into favourable zones and the design of a fracture-dominated utilization approach.

Keywords: Groß Schönebeck, 3D geological modelling, Petrophysical parameterization, Site development, Permian, Elbe reservoir, Permo-Carboniferous volcanic rocks

Introduction

The planning of the overall exploitation concept for low-enthalpy geothermal resources strongly depends on both regional and local geology and includes the drill path design (directional drilling, deviation) and stimulation operations in case of low-productive reservoirs (e.g., von Hartmann et al. 2015; Kana et al. 2015; Ricard et al. 2016). For the development of an adequate (site-specific) exploitation strategy, knowledge on the existence and orientation of large-scale faults, fracture networks and of a possible compartmentalization of target horizons are of utmost importance (c.f., Bunes et al. 2014; Krawczyk et al. 2015). Imaging these structural features at depth and including this knowledge in reservoir models greatly expands the basis for an efficient use of geothermal energy (e.g., Bauer et al. 2010; McGuire et al. 2015).

Among the sedimentary basins worldwide that contain deep geothermal resources (Mendrinós et al. 2010; Pussak et al. 2014; Siler et al. 2016; Zhang and Hu 2018), the North German Basin is one of the three type locations in Germany that offers potential for geothermal heat production. At the Groß Schönebeck research platform, reconnaissance boreholes and vintage 2D seismic lines were lately supplemented by 3D reflection seismic (Krawczyk et al. 2019) and VSP (Henninges et al. 2021; Martuganova et al. 2022) surveys, which provide the basis of the new geological and reservoir model presented in this manuscript.

We address the development of a new site model for the Groß Schönebeck geothermal research platform that shows how already existing knowledge and adapted procedures can help developing a site for geothermal use. For the North German Basin type lithologies, covering Carboniferous to Cenozoic units, we provide reservoir model parameterization of the Permo-Carboniferous target zones that are important for future deep geothermal development. The knowledge and the data sets gained at Groß Schönebeck will also help planning exploitation concepts for comparable geological settings.

Summary of operational site development at Groß-Schönebeck

The research platform Groß Schönebeck is located 40 km north of Berlin (Fig. 1) and was established over the last two decades. The target horizons for geothermal utilization were the sedimentary Permian and the Permo-Carboniferous volcanic rocks, hosting in-situ temperatures of about 150 °C. The site development started with the re-opening of a non-successful 4.2-km-deep hydrocarbon exploration well in 2001 (the E GrSk 3/90 well, which was drilled in 1990) and was followed by initial hydraulic tests and the drilling of a new geothermal research well (the Gt GrSk 4/05 borehole, completed in 2006 as production well). Hydraulic stimulations were performed to increase the fluid inflow to the Gt GrSk 4/05 borehole. Further tests including the installation and operation of a

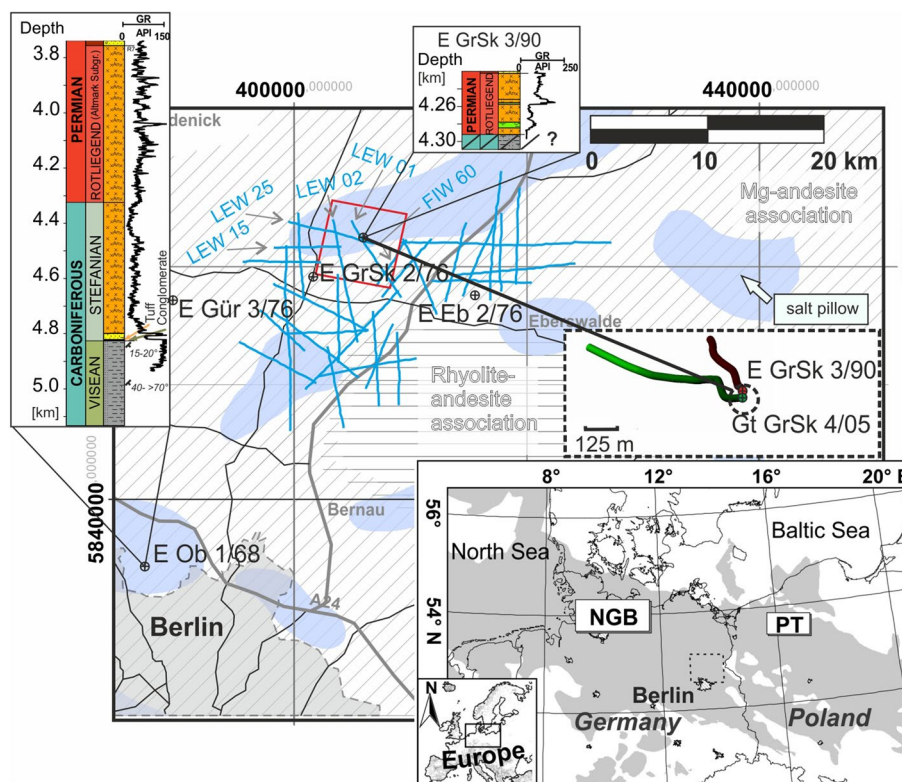


Fig. 1 Site map of Northeast Brandenburg showing the 3D seismic of the Groß Schönebeck study area (red rectangle), the location of former 2D seismic reconnaissance lines (LEW; blue lines), the location of deep boreholes, the distribution of the Permo-Carboniferous volcanic rock associations after Benek et al. (1996), the Permo-Carboniferous succession as encountered in two boreholes (E Ob 1/68 and E GrSk 3/90 based on drilling reports, for legend see Fig. 2), the distribution of salt pillows (blue areas) in the subsurface according to the Northwest-European Gas Atlas (Lokhorst 1998), and main roads and towns (33UTM-WGS84 projection). For orientation, an overview map shows the distribution of Rotliegend sediments (grey shaded) and the location of the study area (stippled rectangle). *NGB* North German Basin, *PT* Polish Trough

geothermal loop followed. The pumping of the high-saline reservoir fluids successively depicted obstacles which hindered a lasting operation of the geothermal loop and thus the commissioning of a heat conversion plant (see summary in Blöcher et al. 2016).

So far, the geothermal exploitation concept relied on a matrix-dominated approach, and sparsely distributed 2D seismic profiles (acquired in 1987, Fig. 1, Table 1) were used to set up a first 3D geological model of the Groß Schönebeck area, forming the base of the first exploitation concept and the well design of the Gt GrSk 4/05 borehole (Moeck et al. 2009). To conclude, the experiences made with this concept were not successful. As an alternative, a concept based on an engineered fracture-dominated exploitation approach for establishing a continuous and sustainable geothermal loop came into discussion. To exclude any structural obstacles, a 3D seismic exploration campaign was performed to shed light into the detailed structural setting of the site. The processing and a first rough interpretation of these data are provided in Krawczyk et al. (2019), while the detailed geological interpretation of the seismic data is part of this paper. The first time determinants for further field development at the site could be identified: formerly hypothesized crustal-scale faults, indications for free gas, seismic compartmentalization in the sub-salinar, and a fracture-dominated Rotliegend reservoir were all not proven

Table 1 Data used in this paper

Kind of data	Name(s)	References
Boreholes—stratigraphy and main lithology	E Ob 1/68, E GrSk 2/67, E GrSk 3/90, Gt GrSk 4/05	drilling reports, partly published in: Hoth et al. (1993), Rockel and Hurter (2000), Holl et al. (2005)
Boreholes—petrophysical rock analysis (cores)	E GrSk 3/90	Rockel and Hurter (2000), Trautwein (2005), Blöcher et al. (2016), Lotz (2004), this paper
Boreholes—geophysical well logging	E GrSk 3/90, Gt GrSk 4/05	Huenges and Hurter (2002), Huenges and Winter (2004)
2D seismic	FIW–LEW: Finowfurt–Liebenwalde campaign, acquired in 1987	König and Meyer (1988); this paper
DAS–VSP data of Groß Schönebeck	Different lines and volumes	Martuganova et al. (2022)
3D seismic of Groß Schönebeck	PoSTM, NMO Stack, CRS-Stack, CRS-PoSTM, PreSDM-DeMultiple (in time and depth domain)	Acquisition in Krawczyk et al. (2019); interpretation: this paper

For location of boreholes see Fig. 1

Abbreviations of different processed seismic volumes: *PoSTM* post-stack time migration, *NMO* normal move out, *CRS* common reflection surface, *PreSDM* pre-stack depth migration, *DeMultiple* suppression of seismic multiples

(Krawczyk et al. 2019). Rather, the seismic facies diversity of the reservoir target units, deduced from a seismic attribute study (Bauer et al. 2020), leads to the interpretation of a system of thicker paleo-channels deposited within a deepened landscape, allowing large-scale thickness variations.

These findings influence the geothermal exploitation concept, so that we present here an in-depth reservoir investigation of the structural setting, including the interpretation of seismic horizons, involved fault systems, and a more complex, geologically based (facies-driven) distribution of petrophysical properties for the reservoir targets.

Geological setting

The Groß Schönebeck deep geothermal research platform is located in the North German Basin (NGB) which is part of the Central European Basin System reaching from Middle England to North Germany, Poland and the Baltic States (Fig. 1; Ziegler 1990; Doornenbal and Stevenson 2010), reflecting a low-enthalpy geothermal setting. The basin developed in the late Carboniferous and early Permian in response to thermal relaxation, crustal extension and tectonic subsidence (van Wees et al. 2000). The subsequent sedimentation resulted in the deposition of sedimentary rocks with a thickness of up to 6.500 m in the eastern part of the NGB (Hoth et al. 1993; DEKORP-BASIN Research Group 1999). The NGB was like other sub basins of the Permian Basin System a target area for the hydrocarbon industry. Several seismic campaigns and deep drillings were performed to investigate the most prospective target zones, like the Permian Rotliegend sediments, also in northeast Brandenburg (Fig. 1). The geological evolution of the basin and its lithological composition will be summarized shortly in the following.

Pre-Permian basement and Permo-Carboniferous volcanic rocks

In the study area (Fig. 1), details on the Carboniferous and pre-Carboniferous basement are not well constrained. Devonian rocks are proven to be partly absent in the

sedimentary succession (Belka et al. 2010) and are indeed not drilled by any deep borehole in Brandenburg (Franke 2015a), although they may be expected in depths of more than 6–7 km. Maximum drilled depths to about 5.2 km give evidence of Lower Carboniferous (Dinantian) rocks in Brandenburg. The rocks encountered consist of fine-grained to coarse-grained greywacke, siltstones and pelites of a distal to proximal flysch facies type (Kopp et al. 2004; Kombrink et al. 2010; Franke 2015b). These deposits of the Carboniferous “Kulm” facies are characterized by a variable dipping of 0–90° and are strongly fissured due to the Variscan orogeny (the Visean of the E Ob 1/68 borehole, Fig. 1). During Permo-Carboniferous times, Brandenburg was part of a back-arc extension regime of the Variscan foreland. In the Westphalian, there was in contrast to the coal-bearing deposits of large areas of Northwest Europe, non-sedimentation in the study area (Kombrink et al. 2010). Due to the progressing thermal subsidence of the evolving extensional regime, the Permian Basin System developed. As a first consequence, an intense volcanic activity resulted in thick successions of Permo-Carboniferous volcanic rocks (Fig. 1). These volcanic sequences do often represent a kind of magmatic basement filling of the sedimentary NGB. According to Breitzkreuz and Geißler (2015), Mg-andesitic rocks dominate in the East Brandenburg Sub Province (Geißler et al. 2008). About 48 boreholes encountered the volcanic succession, but only 10 drilled the volcanic complex completely in East Brandenburg. As described by Benek et al. (1996) and Geißler et al. (2008), the Permo-Carboniferous volcanic succession is characterized by different mineralogical composition and variable rock texture according to the magma, eruptional type and stage, whereby two of five eruptional stages are present in East Brandenburg. The oldest volcanic rock units of the first eruption stage consist of dacitic rocks, followed by lower basaltic andesitic rocks, rhyolitic rocks and middle and upper basaltic andesitic rock units. In East Brandenburg the volcanic succession ends with trachytic rocks of the early phase of the second eruption stage in the lowermost Asselian (Benek et al. 1996). The andesitic rocks do predominate the entire succession and built up to 80% of the total volcanic rock (Huebscher 1995). The andesites are commonly porphyritic consisting of plagioclase, orthopyroxene and olivine (Benek et al. 1996). According to Benek et al. (1996) the entire andesite complex averages a thickness of 200–500 m with a local maximum thickness of more than 1000 m at shield volcanos (E Ob 1/68 well, Fig. 1). Based on their analysis, an initial thickness of about 200 m could be expected for the Groß Schönebeck area.

Middle European Permian (Dyas)

Sedimentary Rotliegend

During the Permian, the subsidence of the NGB causes the deposition of large volumes of sedimentary rocks. In Brandenburg, the primary source rocks of these Rotliegend sediments were the thick andesitic rock sequences. Carboniferous rocks were, although often separated by an unconformity from the Rotliegend sediments, not source rocks of the deposits (Rieke 2001). The high altitude areas of the volcanoes were eroded and deposited in braided plain and aeolian to fluvial environments at the basin margin and in sand flat and mud flat environments at the distal areas of the basin centre. Different subsequent climatic and tectonic events trigger basin-wide traceable sedimentary cycles in the Rotliegend with sequences of thicknesses of 20–100 m (Rieke et al. 2003). The cycles

often start with clay/mud-dominated horizons (highstand) and evolve to more regressive sediments (shoreface and deltaic sands toward the top which progrades laterally into offshore shales, lowstand) and end with the next maximum flooding surface (highstand; Gast 1995). According to Gebhardt et al. (1991), tectonic events are the main cause for the development of the fining-upward cycles of the Parchim, Mirow, Dethlingen und Hannover Formations. The climatic conditions during the Rotliegend were semi-arid to arid, causing the dominating Fe-oxidized reddish colour of the deposits.

The area of Groß Schönebeck is situated in a SE marginal position of the NGB. Here, clast supported coarse-grained conglomerates and sandstones of the Havel Subgroup cover the Permo-Carboniferous volcanic rocks (E GrSk 3/90 borehole, Figs. 1 and 2). Holl et al. (2005) interpreted these deposits as fluvial sediments of coarse-grained bed-load rivers in a braided plain environment. In the E GrSk 3/90 borehole, the multistoried channels were deposited in a NNE to NW striking depositional system with a mean paleocurrent direction of 24° for the Lower Havel Subgroup and 340° (NW) for the Upper Havel Subgroup (Holl et al. 2005). By the end of the Havel Formation, the landform configuration changed fundamental. Due to thermal subsidence, the North-German trough extended further to the west reaching the Netherlands and England (Gast and Gebhardt 1995). The rise of the hinterland allows the development of erosive sandy deposits, which cover the entire southern margin of the NGB. These quartz-dominated sandy deposits represent one of the geothermal reservoir target, the Elbe reservoir sandstone (ERS) that is equivalent to the so-called *Elbebasissandstein* (EBS) of Bauer et al. 2020.

The ERS is well documented in boreholes along the marginal areas of the NGB (Fig. 2 and Gast et al. 1998; McCann 1998). Stratigraphically, the ERS comprises parts of the

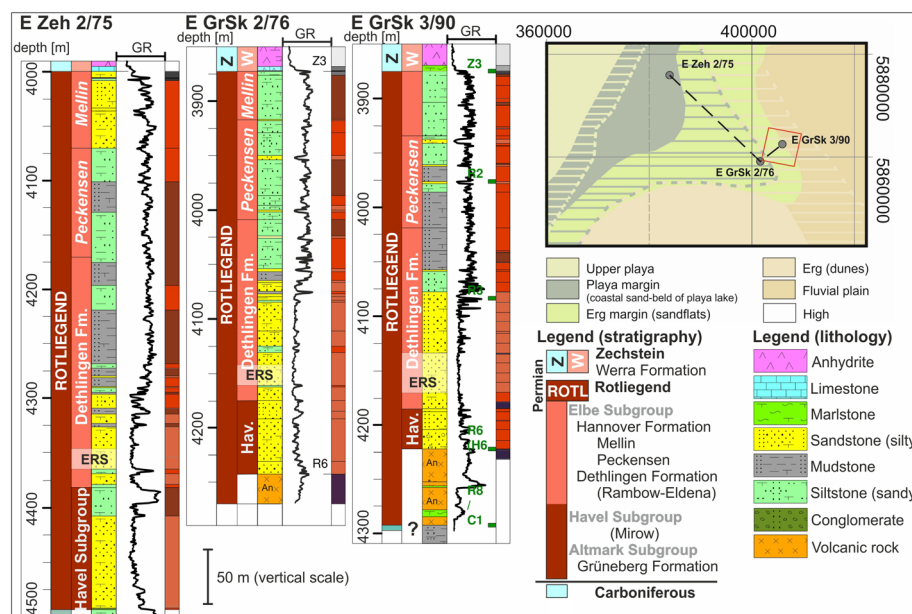


Fig. 2 Rotliegend in East Brandenburg (Groß Schönebeck) as encountered in selected boreholes (interpreted from drilling reports) and respective facies interpretation according to Doornenbal and Stevenson (2010; inset map). ERS marks the sedimentary geothermal target (Elbe reservoir sandstone). GR are gamma-ray log readings for correlation (partly digitized)

Dethlingen Formation, the Hannover Formation, and possible parts of the Mirow Formation (Fig. 2). The ERS shows a variable thickness of up to about 200 m near the coastline (Lindert et al. 1990) and thins out toward the basin centre. Many samples of the ERS show a bimodal grain-size distribution. Plein (1995) interprets the sandstone to represent sand that was accumulated under aeolian conditions of the hinterland first before it was transported by aquatic processes toward the basin and lithified. In the E GrSk 3/90 well, the ERS shows a thickness of about 40 m within the Dethlingen Formation (Bauer et al. 2020, sandstone interval with low GR intensity in Fig. 2). According to Holl et al. (2005), the fine-to-coarse-grained sandstones were deposited in an ephemeral stream floodplain environment. The palaeocurrent direction distribution is more variable than in the Havel Subgroup but is still to the NW (mean azimuth: 290°; Holl et al. 2005). In open-hole logs, the ERS is characterized by low gamma-ray values and shows a high quartz content. In addition, decreased P-wave velocities observed by sonic logging indicate an increase of porosity (Trautwein and Huenges 2005). These two observations explain the general interest in the ERS as a geothermal target, hosting water of about 150 °C temperature in Groß Schönebeck (Huenges 2002).

Within Rotliegend times, the sedimentation regime in the central area of the basin got more and more influenced by cyclic fluctuations of the water table, and a growing salt lake developed from the central part of the basin (Gast and Gebhardt 1995). A progressive planation of the morphology in combination with the reduction of sediment supply resulted in the development of sediments of the mud flat facies. The playa deposits cover large parts of the NGB during the late Rotliegend (Rieke et al. 2001; Gast et al. 2010). This is also the case in Groß Schönebeck, where mudstones do predominate the lithology of the Hannover Formation, partly interrupted by sandy deposits of a sandy mudflat environment.

Zechstein

During the Late Permian, the basin developed into an intracontinental topographic depression which was rapidly flooded by a catastrophic transgression from the Barents Sea (Peryt et al. 2010; Strozyk et al. 2017). In many areas, the uppermost 10–15 m of Rotliegend sandy sediments were reworked and form the Weissliegend which locally grades into limestone and is overlain by the Kupferschiefer (Peryt et al. 2010). Subsequently, cyclic occurring flooding events lead to the deposition of 1500–2000 m of Zechstein deposits reflecting progressive evaporation (e.g., Zhang et al. 2013). The cyclicity is represented by the Zechstein deposits consisting of transgressional carbonates and mudstones followed by evaporates (Peryt et al. 2010). The nowadays thickness of Zechstein deposits is very variable and triggered by post-Permian salt movement (salt tectonics) and erosion (see later in text). In Groß Schönebeck, which is located on top of a salt pillow, the Zechstein sequence shows a total thickness of approximately 1500 m.

Post-Permian deposition and evolution of salt structures

In the late Permian, a phase of accelerated subsidence commenced because of thermal contraction and continued until the end of the early Triassic in the NGB. Since then, subsidence rates were decreasing exponentially according to a thermal subsidence pattern (Scheck and Bayer 1999). Only for time intervals in the late Triassic as well as the

late Cretaceous and Cenozoic, the subsidence rates were accelerated again, varying spatially in magnitude within the basin (Scheck and Bayer 1999; Kossow and Krawczyk 2002). In the mid-to-late Triassic, the thinning of supra-salt sediments due to an extensional regime in conjunction with subsidence caused instabilities of the Zechstein salt deposits and initiated the formation of salt structures (Kossow et al. 2000; Scheck-Wenderoth et al. 2008). In the late Cretaceous to earliest Cenozoic, salt diapirism was associated with compression (Scheck et al. 2003). After this compressive phase, the Cenozoic subsidence phase enabled further intensive salt movement. In relevant areas, Pleistocene glaciations may have triggered still active salt movements due to the loading and unloading of ice sheets (Strozyk et al. 2017).

German Triassic (*Buntsandstein, Muschelkalk, Keuper*)

The deposits of the *Buntsandstein* form the first sediments above the Zechstein. Still arid conditions with fluvial sedimentation did prevail during that time (Stackebrandt and Röhling 2015). Only the Middle *Buntsandstein* shows higher depositional energies resulting in a higher and coarser-grained sand content, while the Lower and Upper *Buntsandstein* consists of fine-grained (clayey) sediments. The coarser-grained sandy deposits within the Volpriehausen, Dethfurt, Hardegsen, and Solling Formations (Middle *Buntsandstein*) are often discussed as possible geothermal reservoirs. At Groß Schönebeck, the thickest sandstone interval occurs in the Dethfurt Formation with a thickness of 10 m, showing a cleaner sand interval of about 6 m and temperatures of 85 °C at a depth of 1870 m. The ingress of marine conditions in the Upper *Buntsandstein* and the forming of evaporates resulted in basin-wide traceable impedance contrasts in the lithological succession and in prominent seismic markers (S1 and S2, Fig. 3).

In the *Muschelkalk*, the NGB was connected in the south with the Tethys Ocean and formed an epicontinental flat sea. Calcareous sediments such as marlstones and limestones do represent the predominant lithotypes of this time. The *Muschelkalk* is divided in three subunits (Lower, Middle, and Upper). In the Lower *Muschelkalk*, oolitic limestones of the so-called *Wellenkalk* could represent a potential geothermal reservoir if fractured and appropriate fluid paths are present. In Groß Schönebeck, the E GrSk 3/90 borehole did not observe any fluid flow in this succession during drilling. Temperatures of 70 °C are measured in the respective depth interval (1500–1550 m). In the Middle *Muschelkalk*, the connection to the Tethys was sporadically closed, resulting in the formation of evaporitic sediments. Basin-wide traceable seismic marker horizons are connected to this event (M1 and M2, Fig. 3).

The *Keuper* represents the Upper German Triassic. *Keuper* sediments are predominantly characterized by fine-grained deposits of the stillwater facies, of fluvial facies, and subordinate of marine facies. Based on basin-wide recognizable discontinuities, the *Keuper* is subdivided in several formations (Fig. 3, e.g., Beutler and Franz 2015). Depending on the respective lithological composition and succession, the discontinuities are partly related to more or less pronounced seismic reflectors (K1, K2, Fig. 3). According to Beutler and Franz (2015), the unconformity at the boundary of the Grabfeld Formation and the Stuttgart Formation was related to tectonic events which also causes the first salt diapir forming phase. The salt structure of Groß Schönebeck formed

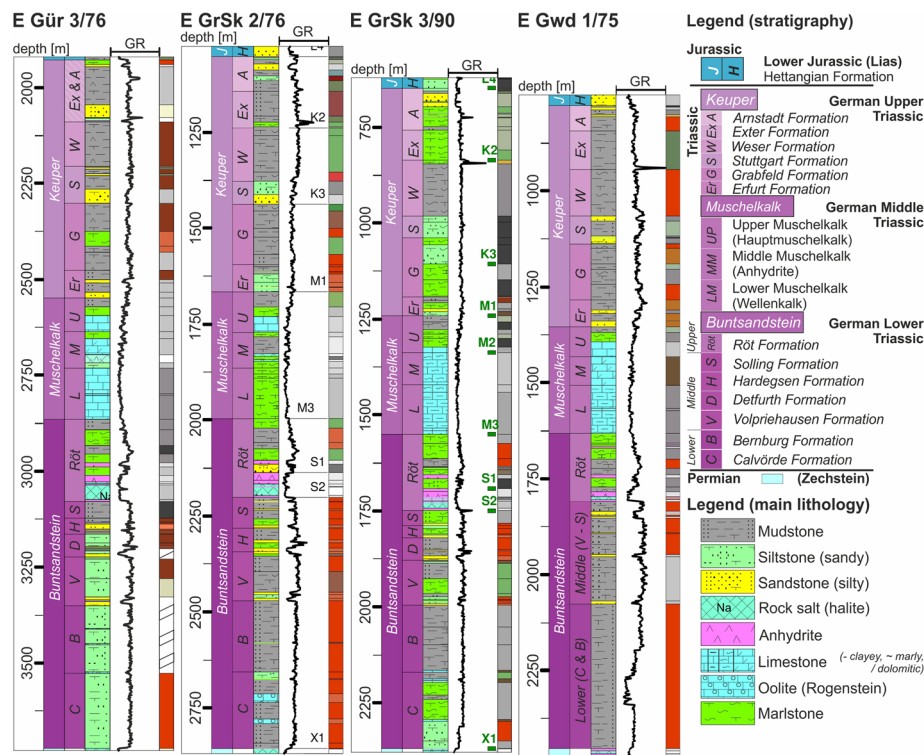


Fig. 3 German Triassic deposits (thickness, lithological composition, and prevailing rock colour) as encountered in boreholes in East Brandenburg, interpreted from unpublished drilling reports. For location of boreholes, see Fig. 1. GR are gamma-ray log readings for correlation (partly digitized)

during Keuper times and represents a salt pillow with only minor hiati of less than 30 m (Beutler and Franz 2015).

Jurassic, Cretaceous and Cenozoic

The movement of salt during the Upper Triassic causes the formation of troughs and highs and affects post-Triassic sedimentation and erosion processes. For Groß Schönebeck, only Lower Jurassic (Northern Lias Group) sediments are present in the drillings on the salt pillow (Fig. 4). The deposits represent marine shale facies and are partly interfingering with shallow-marine sands and limnic and terrestrial sediments. The change of lithological composition due to different facies conditions allow the mapping of several seismic horizons with variable reflectivity (L2 and L4, Fig. 4).

During most of Lower *Cretaceous* times, almost the complete area of East Brandenburg was part of a structural high without any preserved sediments. Finally, the highland of East Brandenburg became part of a marine depositional environment, which continued to the Upper Cretaceous. Depending on the particular structural situation (paleogeography), respective sediments were deposited (e.g., E GrSk 2/76, Fig. 4).

In the *Tertiary*, large parts of the NGB became flooded. Marine clayey sediments of the Oligocene (the Rupelian “Rupelton”) document the basin-wide marine transgression of the paleo-North Sea. In salt rim synclines, the Tertiary could achieve a much greater thickness (see E Gür 3/76, Fig. 4). Changing water tables and coastline conditions in the Miocene allow the formation of coal beds (lignite) in southeast Brandenburg. In the late

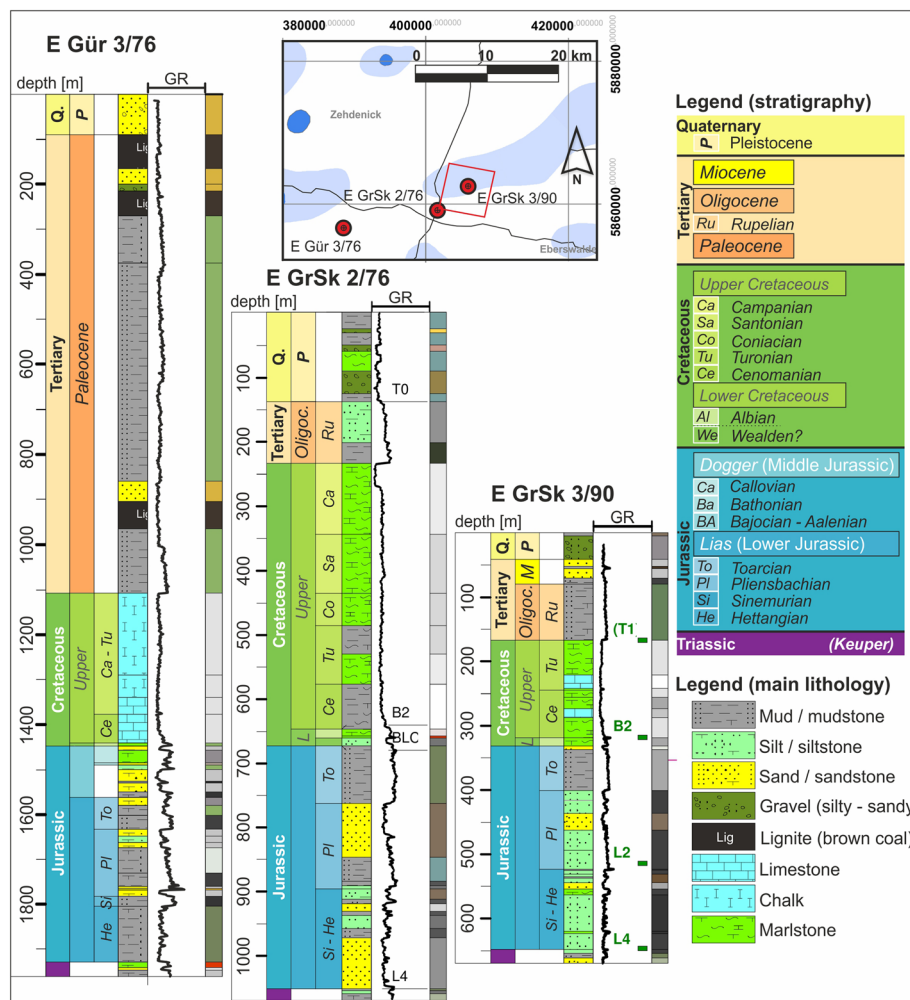


Fig. 4 Jurassic, Cretaceous and Cenozoic deposits (thickness, main lithological composition and prevailing rock colour) as encountered in the Grüneberg (E Gür 3/76) and Groß Schönebeck (E GrSk 2/76, E GrSk 3/90) boreholes in East Brandenburg (interpreted from unpublished drilling reports; GR are gamma-ray log readings for correlation, partly digitized)

Tertiary (Middle Miocene to Pliocene), the marine conditions in Brandenburg vanished owing to another regression. Therefore, sediments of that age are almost not present in northeast Brandenburg.

The *Quaternary* deposits are dominated by glacial sediments of the different ice ages (boulder, sand, clay, till, Fig. 4). They host the main fresh water resources. Due to glacial troughs that cut into the underlying strata and allow the deposition of glacial sediments, the Quaternary thickness could vary significantly on short distances.

Data and methods

The presented study integrates various types of subsurface data, covering different scales and different qualities that are shortly addressed in the following (Table 1). The data were evaluated and used to establish a new geological model of the site and to allow a more realistic parameterization of the Permo-Carboniferous reservoir target. Petrophysical

properties to be considered in the facies-depending modelling are total and effective porosity, density, permeability and thermal properties (thermal conductivity, thermal diffusivity, heat capacity).

Literature and map data

For regional correlation, the geological atlas of Brandenburg (Stackebrandt and Manhenke 2010), providing different thickness and depth maps of units of the Mesozoic and Cenozoic was used. In parts, former synopsis representations of legacy exploration data for facies and structural interpretation could be used (e.g., Lange et al. 1981; Doornenbal and Stevenson 2010).

Borehole data and evaluation of petrophysical properties

Mainly due to the efforts of the hydrocarbon exploration in the time period of 1960–1990, several deep drillings provide valuable underground information and are available for cross-correlation (Hoth et al. 1993). In the Groß Schönebeck area, the E GrSk 2/68 borehole, the E GrSk 3/90 borehole, which was deepened about 50 m without coring in 2001 as a geothermal well, and the Gt GrSk 4/05 geothermal well provide unique access to underground data (Fig. 1, Tables 1 and 2). Of special interest are the geophysical logging data, still available cores (E GrSk 3/90), the respective drilling reports, and petrophysical measurements for correlation and petrophysical interpretation and parameterization of the model (Table 2). To extend the data basis, available cores were studied in the repository and additional samples were taken for the determination of thermal properties. The core and log data used in this study is provided by a data publication to this manuscript.

Table 2 Data and material of the E GrSk 3/90 and Gt GrSk 4/05 boreholes

a) Core data (E GrSk 3/90 only; coring in Gt GrSk 4/05 was planned but could not be realized). The E GrSk 3/90 borehole was cored in the depth range of ca. 4040–4270 m (230 m). Due to disposal of core material in the late 1990s, only the lowermost 63 m of this section are still available in the repository		
Density and porosity	In total 344 measured samples: 287 legacy samples (Hamann et al. 1991), 29 samples (Trautwein 2005), 17 samples (Lotz 2004), 11 samples (this study)	
Gas permeability	In total 137 measured samples: 109 legacy samples (Hamann et al. 1991), 28 samples (Trautwein 2005) plus 3 measured under in-situ conditions (Trautwein 2005)	
Thermal conductivity	Lotz (2004); Norden et al. (2022)	
Thermal diffusivity	Norden et al. (2022)	
b) Well logging		
Stratigraphy	E GrSk 3/90	Gt GrSk 4/05
Post-Rotliegend	Gamma-ray (GR)	GR
Prae-Zechstein	GR	GR, Spectral GR
	Temperature log	logging tools used for correlation
	Sonic/velocity log	only due to inconsistent quality
	Bulk density log	(mineral detection, dual laterolog,
	Neutron porosity log	monopole acoustic)
	Pulsed neutron log	
	Electrical image log	

The data used in this paper are available in a data publication to this manuscript (Norden et al. 2022)

Geophysical logging data

By working with the well-logging data it soon became obvious, that the data of the E GrSk 3/90 borehole and especially of the Gt GrSk 4/05 borehole needed a depth correction based on a consistent depth reference log covering the complete drilled sequence. Therefore, a master gamma-ray log was chosen from the E GrSk 3/90 and used for depth calibration. This enabled a consistent interpretation of the drilled lithological and stratigraphical units for the two close-by boreholes. In the E GrSk 3/90, beside an undisturbed temperature log, an acoustic, a density, a neutron, and an electrical image log was measured in the Rotliegend reservoir section (Table 2). The latter was used for an analysis of depositional structures (Holl et al. 2005). Based on the work of Holl et al. (2005), an analysis of the sedimentary dip azimuths using the azimuth-vector plot method (after Rider 2000) was applied in the current study. For this method, dip azimuth values are plotted sequentially in their true orientation but without any depth scale. Dip azimuth changes due to different sedimentary regimes will result in different line orientation.

Permeability could be deduced from a pulsed neutron log that was measured over parts of the sedimentary reservoir section. Permeability was additionally estimated for the sedimentary Rotliegend based on the approach of Coates et al. (1991) according to

$$k = a \cdot \Phi^b \cdot \left(\frac{F}{B}\right)^c, \tag{1}$$

where k is permeability, Φ is total porosity, B is bound fluid volume (calculated as the product of the volume of clay, V_{Cl} , and the clay total porosity, Φ_{Cl}), F represents the free fluid volume ($F = \Phi - B$), and a, b, c are empirically derived constants. The Coates equation is fitted to laboratory permeability data, corrected for in-situ conditions, by manually adjusting the constants a, b , and c (see later in text).

For a first evaluation of permeability of the volcanic rock sequence, we used a correlation based on core investigations given by Siratovich et al. (2014) for andesitic rocks of the Taupo Volcanic Zone in New Zealand. They establish a relation between connected porosity (PHI) and permeability (PERM) for the Rotokawa andesite that we applied to our data. The porosity needed in the calculation was estimated from the respective sonic log (Table 2) using the Wyllie time-average equation (Wyllie et al. 1956).

The thermal conductivity (TC) for the igneous rock section was determined using the empirical approach of García et al. (1989) developed for andesitic rocks of the Los Azufres geothermal field in Mexico. They used TC measurements under ambient conditions on low-porosity dry core samples, showing similar values as on andesitic samples of the Northeast German Basin, and correlate them with porosity and bulk density (BD) data according to the following formula:

$$\log_{10} \left(TC \left[\frac{W}{mK} \right] \right) = \left(3.7221159 - 0.00472402 * PHI[\%] - 0.000594151 * PHI[\%]^2 \right) - \log \left(BD \left[\frac{kg}{m^3} \right] \right) \tag{2}$$

To apply their approach on the log data of E GrSk 3/90, we rely on the above calculated porosity from the sonic log and use the sonic also for the density estimation. Instead of

Table 3 Seismic horizons mapped in the new Groß-Schönebeck 3D seismic data set, calibrated with borehole data

Reflector	Horizon	Reflector quality	Stratigraphy
B2	Near base of Upper Cretaceous	Weak (uncertain)	CRETACEOUS
BLC	Near base of Lower Cretaceous	Weak	
L2	Within Jurassic (Pliensbachian)	Variable	JURASSIC
L4	Near base of Lower Jurassic	Strong	<i>Lias</i>
K2	Near top of Weser Formation	Variable (uncertain)	TRIASSIC
K3	Near top of Grabfeld Formation	Well developed	<i>Keuper</i>
M1	Near top of Middle Muschelkalk	Strong	TRIASSIC
M2	Within Middle Muschelkalk (anhydrite)	Well developed	<i>Muschelkalk</i>
M3	Near base of Mittlerer Muschelkalk	Strong	
S1	Within Röt Formation (top of anhydrite)	Strong	TRIASSIC
S2	Near base of Röt Formation	Strong	<i>Buntsandstein</i>
X1	Near top of Zechstein	Strong	PERMIAN
X3	Near basal anhydrite (Leine Formation)	Strong	<i>Zechstein</i>
Z1	Near top of basal anhydrite (Staßfurt Fm.)	Very strong	
Z3	Near base of Zechstein	Well developed	
R3	Within Dethlingen Formation	Variable (uncertain)	PERMIAN
Top ERS	Near top of Elbe reservoir sandstone	Variable (uncertain)	<i>Rotliegend</i>
Base ERS	Near base of Elbe reservoir sandstone	Well developed	
R6	Near base of sedimentary Rotliegend	Well developed	
R8	Near base of volcanic succession	Very weak (uncertain)	PERMOCARBONIFEROUS

Reflector names are according to Reinhardt (1993)

using the Gardner’s relation (Gardner et al. 1974), which is commonly applied for sedimentary rocks, we used the provided measured properties of Siratovich et al. (2014) to establish a specific correlation of sonic velocities and BD for andesitic rocks:

$$BD \left[\frac{\text{kg}}{\text{m}^3} \cdot 10^3 \right] = 0.0278 \cdot \text{Sonic} \left[\frac{\text{m}}{\text{s}} \right]^{0.5404}, R = 0.63. \tag{3}$$

Specific heat capacities (SHC) of the volcanic rock section were calculated using a formula provided by Heap et al. (2020), developed for andesitic rocks of Mt. Ruapehu in New Zealand based on porosity, bulk and matrix density:

$$\text{SHC} \left[\frac{\text{J}}{\text{kgK}} \right] = \frac{2750 \left[\frac{\text{kg}}{\text{m}^3} \right] \cdot 750 \left[\frac{\text{J}}{\text{kgK}} \right] \cdot (1 - \text{PHI}[\text{dec}]) + 1000 \left[\frac{\text{kg}}{\text{m}^3} \right] \cdot 4182 \left[\frac{\text{J}}{\text{kgK}} \right] \cdot \text{PHI}[\text{dec}]}{BD \left[\frac{\text{kg}}{\text{m}^3} \right]} \tag{4}$$

Because both approaches (for TC and SHC estimates) provide ambient values, not considering in-situ pT conditions, corresponding corrections were applied. The TC correction was calculated as a summary effect of single corrections on TC for the respective *p* and *T* conditions (TC_p and TC_T, respectively).

The *p* effect on TC of magmatic rocks (TC_{pm}) was considered based on the equation of Fuchs and Förster (2014) and the *T* effect on TC (TC_{Tm}) was corrected following the

approach of Sekiguchi (1984), adapted for T in °C, TC in $Wm^{-1} K^{-1}$, and ambient T of 20 °C (293.15 K) instead of 15 °C (288.15 K).

Waples and Waples (2004) provide a comprehensive review on SHC of rocks, minerals, and subsurface fluids. They conclude that p corrections on SHC of solids can be neglected. Therefore, SHC was corrected for T following the procedure given by Waples and Waples (2004).

The in-situ thermal diffusivity ($TD_{in-situ}$) finally was calculated based on the corrected thermal conductivity and heat capacity values and the estimated bulk density according to

$$TD_{in-situ} \left[\frac{m^2}{s} \right] = \frac{TC_{in-situ} \left[\frac{W}{mK} \right]}{BD \left[\frac{kg}{m^3} \right] \cdot SHC_T \left[\frac{J}{kgK} \right]} \quad (5)$$

See data publication for details on the calculations.

Core data

The petrophysical data compilation includes density, porosity, permeability, thermal conductivity, and thermal diffusivity of different core samples from the E GrSk 3/90 borehole, measured by different authors (Table 2, also in data publication).

For petrophysical interpretation, the legacy gas-derived laboratory permeabilities of the Rotliegend were corrected taking pressure and brine effects into account using the approach of Juhasz (1986). Juhasz provides correction formulas to correct for three important factors contributing to the discrepancy between routine gas-permeability data and in-situ intrinsic brine permeabilities: (a) gas slippage (Klinkenberg effect; Klinkenberg 1941), (b) absence of confining stress on the sample, and (c) the dry measurement condition of gas permeability measurements (possibly effecting the pore structure). Depending on the value of the measured gas permeability, Juhasz provides different correction formulas that were applied on the laboratory data (the details of the correction procedure are listed in the data publication to this paper).

To enable a better thermophysical characterization of the Rotliegend, additional cores were taken from the core repository, measured, and evaluated for thermal conductivity, thermal diffusivity, and specific heat capacity. The under ambient laboratory-derived parameters were corrected for in-situ pressure and temperature conditions, taking correction functions for sedimentary and magmatic rock types into account (Fuchs and Förster 2014; Somerton 1992; Sekiguchi 1984; Emirov et al. 2017). The data and the applied methodology is presented in the accompanying data publication.

Seismic data

The main input for the structural geological model is the acquired 3D seismic of Groß Schönebeck (Table 2). Main acquisition and processing parameters of this survey are reported in Krawczyk et al. (2019). They provided also a first geological interpretation of the data, but without a detailed analysis and without establishing a geological model. The latter is the focus of the manuscript at hand. For well-tie integration, data from a vertical seismic profile conducted in the E GrSk 3/90 and Gt GrSk 4/05

boreholes with a distributed acoustic sensing system (Henninges et al. 2021) provided important input. The study of Bauer et al. (2020) providing a seismic facies classification on the Rotliegend sandstone reservoir was used to enhance the structural modelling and petrophysical property simulation (e.g., thickness and porosity distribution) for the ERS. The current interpretation of possible reservoir thicknesses of Martuganova et al. (2022) was considered as well. In addition, former legacy 2D seismic surveys in the study area of the 3D seismic were available in a digital format or as georeferenced scanned images for comparison.

Hydraulic data

The reservoir targets, the Permian Rotliegend ERS and the drilled succession of the volcanic rocks were stimulated hydraulically in Groß Schönebeck. Blöcher et al. (2016) describe the details on the stimulation history and respective data (see also references therein). The stimulations provide information on the in-situ hydraulic and mechanical behaviour and the stress regime of the Permian reservoir zones. During stimulation, passive seismic sensing was applied. The recorded microseismic events (Kwiątek et al. 2010) and their in-depth interpretation (Blöcher et al. 2018) provide further information on the reservoir setting and model parameterization showing that at least two of the so far interpreted fault planes would show slip tendencies above a friction coefficient of 0.85. However, there were no seismic events recorded for these planes, implying that the existence of these faults (derived from 2D seismic interpretation) should be questioned (Blöcher et al. 2018).

The available types of underground data were interpreted using the commercial interpretation software Petrel 2016, which was also partly used for seismic analysis, seismic-well tie, horizon interpretation, model building, facies simulation, and petrophysical modelling. Also seismic attribute analysis and visualization techniques were performed in time and depth-domain volumes using the Petrel 2016 software package.

Seismic-well tie and horizon mapping

Seismic-well ties rely on the available logging data and horizon interpretations. For the GroßSchönebeck data, in a first step, composite gamma density and sonic velocity logs were compiled for the depth range of the E GrSk 3/90 borehole (Fig. 5). Because sonic velocity and gamma density were not measured above 2332 m and 3850 m, respectively, this composite log contains logging data from neighbouring wells covering the same stratigraphy and similar lithology and, additionally, for uncovered sections estimated density values. The resulting composite logs should represent at least a realistic sonic/density-distribution scenario for the entire drilled sequence. Additional velocity data were acquired with the DAS technique and provide a direct and robust time-depth relation that was used to calibrate the compositional sonic log. These data are available from a depth of 815 m to about 4250 m, covering one-way travel time and respective (measured and true vertical) depth information with a spacing of 25 m. Based on the calibrated sonic data, a synthetic seismogram was modelled to support the horizon interpretation of the 3D seismic PoSTM data. The depth-converted PreSDM-DeMultiple volume was processed to remove reflection horizon multiples especially for the sub-salt depth

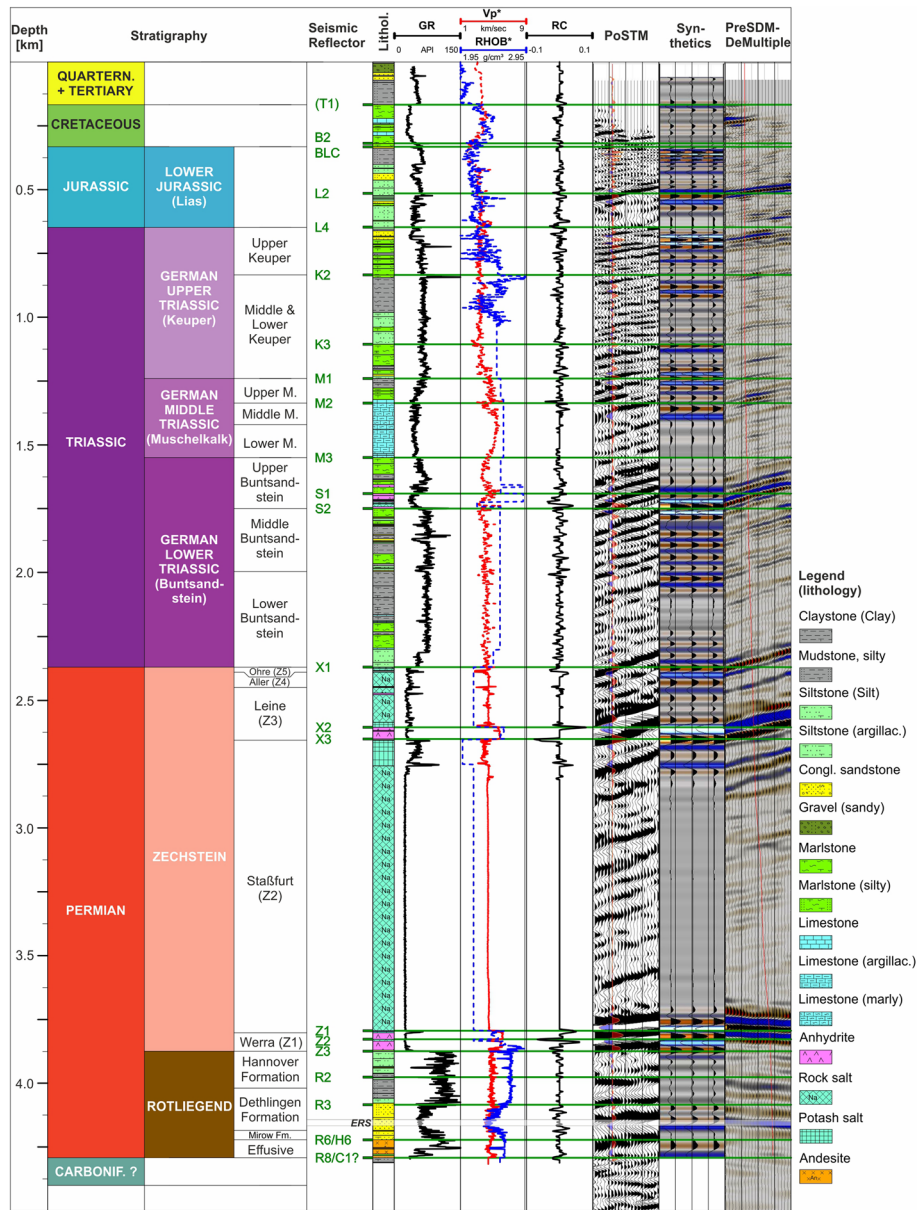


Fig. 5 Seismic-well tie of borehole data (E GrSk 3/90 borehole) and seismic volumes. V_p^* refers to p-wave velocity (in kms^{-1}), RHOB^* to bulk density logging (in 10^3 kgm^{-3} or gcm^{-3}), and RC represents the reflector coefficient, ERS: Elbe reservoir sandstone. The synthetic seismic response based on the applied wavelet is shown together with two processed seismic volumes: PoSTM (post-stack time migration) and PreSDM (pre-stack depth migration with suppression of seismic multiples). Stippled lines of the sonic-density composite plot (V_p^* , RHOB^*) indicate interpolated log responses, see text

domain. For this purpose, a data-driven approach (e.g., Jakubowicz 1998) was applied to predict and subtract undesired interbed multiples before pre-stack depth migration. Horizons interpreted in that volume were later shifted to the respective horizon depth encountered in the boreholes.

The complete suite of seismic horizons and their interpretation in the seismic volume is given in Table 3. The uppermost seismic reflector, which is traceable in the seismic volume, represents the L2 reflector. Reflectors above are fragmentary and hard to follow in the seismic volume. Dominant, continuously developed reflectors are the L2, L4, M2, S1, S2, X1, X2 (X3), and the Z(1–3) reflectors (c.f., Krawczyk et al. 2019). Less pronounced are the reflectors K2, K3, M1, M3, R2, and R6(H6). A distinct reflectivity related to the base of the volcanic rocks (R8/C1) was not observed in the volume.

Structural and lithological interpretation

The focus of the 3D seismic survey aimed at the exploration of the Rotliegend (pre-Zechstein; Krawczyk et al. 2019), so that the seismic survey was optimized for imaging deep targets which results in a lower coverage of the shallower subsurface. The most dominant seismic feature within the data is the Zechstein salt structure. While the sedimentary Rotliegend and the top of the Permo-Carboniferous volcanic rocks were also imaged by the seismic data, deeper Pre-Permian structures are hard to elaborate, the more since related borehole data are absent. Figure 6 shows for one section of the seismic volume the challenges associated with the geological interpretation at salt structures. The seismic processing applied and its visualization affects the overall appearance of reflector continuity and intensity. To improve the correct location of reflection surfaces, the CRS (common reflection surface)-stack-based seismic reflection imaging is providing information that is more reliable (Fig. 6A vs. B, C). Compared with conventional seismic reflection processing, the CRS method (e.g., Mann et al. 1999) provides stacking results with higher signal-to-noise ratio by involvement of more traces from neighbouring CMP (common-midpoint) locations. Moreover, unlike in conventional stacking, the CRS method is based on a purely data-driven design of the stacking operator, which allows an improved imaging of complex

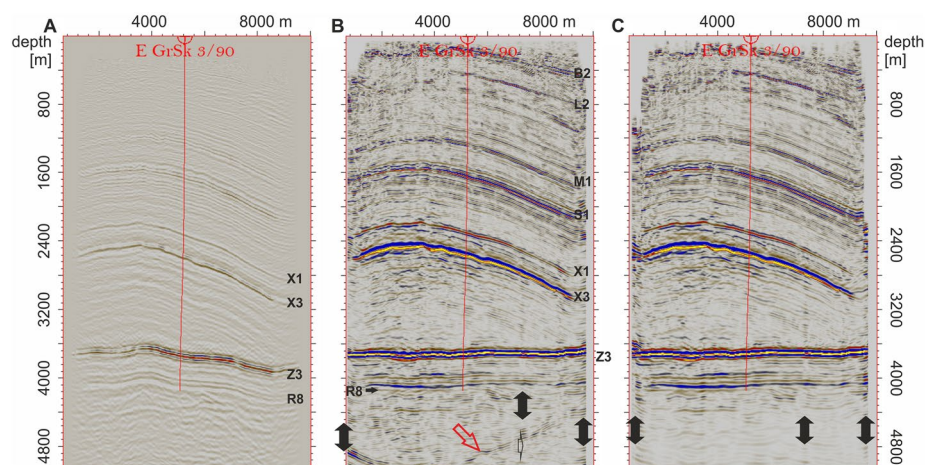


Fig. 6 Depth-converted seismic sections along NW–SE trending profile B (for location see Fig. 7). **A** Post-stack time migration without CRS stack, **B** pre-stack depth migration with CRS stack, **C** pre-stack depth migration with multiple reduction (see also Table 1). Black arrows indicate processing artifacts; the red arrow marks a multiple reflection

geological structures. Due to strong velocity contrasts and changes by the salt doming, the corrections are highly relevant. Reflection multiples of shallower surfaces may also overlay deeper (and weaker) reflections. Processing of the seismic volume by calculation of the behaviour of reflector multiple of main shallow reflectors and subtracting them from the deeper parts of the volume may allow a more precise interpretation (Fig. 6C). However, the complexity of the processing procedure may also introduce (artificial) artefacts like at the edges of the volume and for the trace-like feature visible in Fig. 6B, C.

Pre-Permian and Permo-Carboniferous volcanic rocks

Some local structures and internal features within the pre-Permian are present but hard to relate to a more specific geological interpretation (Fig. 7). The volcanic rocks encountered in the E GrSk 3/90 and Gt GrSk 4/05 boreholes are not well characterized by the seismic volume. Changes in thickness of the volcanic succession or in its chemical composition is not resolved by the seismic data. In profile B and C (Fig. 7), there is an area of increased reflectivity visible in a zone about 1 km east of the GrSk drill site. Remarkably, the profile B shows in that zone a dominant feature with changing polarities (black arrow), probably related to a heterogeneous lithology, a fractured or tilted structures of the Carboniferous or even to processing artefacts rather than reflecting gas-bearing units. Based on the seismic data, at least two scenarios for the base of the volcanic sequence (the top of Carboniferous) are possible. At the supposed top of Carboniferous

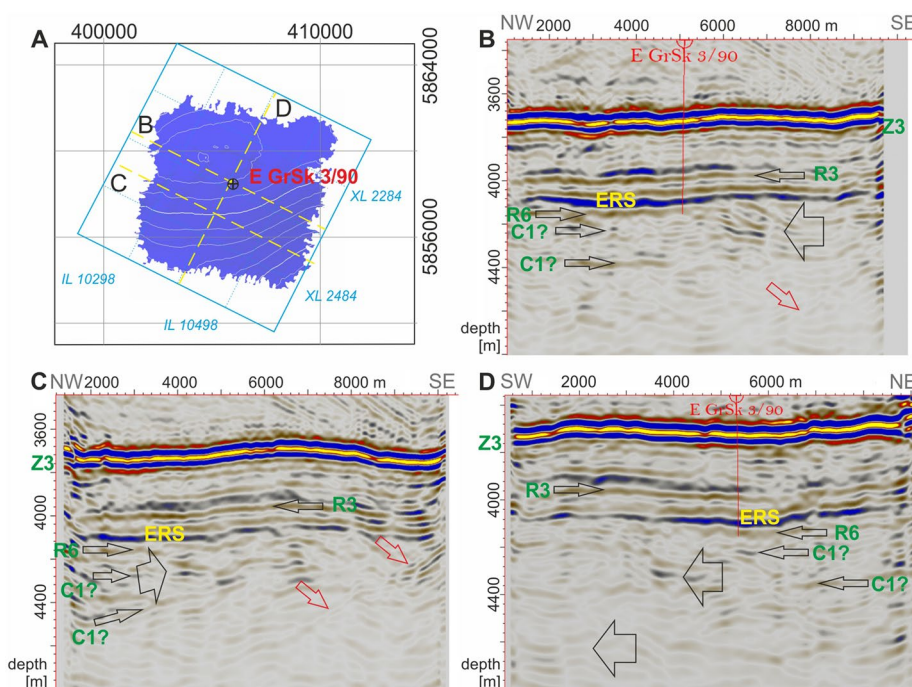


Fig. 7 Seismic cross sections imaging the Rotliegend and pre-Permian at the Groß-Schönebeck site. **A** Locations of the profiles presented and borehole E GrSk 3/90. **B, C** NW–SE sections, **D** NNE–SSW section. The base of the Zechstein salt is evident by the dominant reflector band in all three sections (the lowermost interpreted as Z3). Mainly homogeneous internal reflections within the Rotliegend successions are prevailing (R3, R6, C1), and the Elbe reservoir sandstone (ERS) could be recognized as continuous reflection band. Several internal features occur in the pre-Rotliegend below the base of the Havel Subgroup (R6, black arrows). The red arrows mark seismic multiples

in the E GrSk 3/90 borehole, a weak seismic reflector is more or less traceable in the seismic volume (the upper C1? indication in Fig. 7). However, the lithostratigraphical boundary was indirectly deduced by well-log interpretation, only (Holl et al. 2005), and the interpretation is still under debate. There is a second reflectivity in a depth range of about 4400 m that is often recognizable in the seismic volume. The reflector is beyond well control but could represent an internal reflector within the Carboniferous, or even correspond to a reflectivity related to the top Carboniferous. We mapped both: one referring to a volcanic sequence thickness of about 70 m (Fig. 8A) and another referring to the lower C1 reflector shown in Fig. 7, referring to a thickness of more than 200 m (Fig. 8B).

Permian

While the petrothermal target of the Permo-Carboniferous volcanic rock succession is not very well resolved by the seismic data, the base of the sedimentary Rotliegend, corresponding to the base of the Havel Subgroup for the area of the seismic survey, is related to a seismic reflector in a depth of about 4140 m that is named R6. The R6 reflector (Table 2 and Fig. 7) marks the transition of well-cemented conglomeratic deposits of the Havel Subgroups to the volcanic extrusive rocks and is related often to a zero crossing from negative to positive amplitude change (from lower to higher velocities).

Above the R6 reflector, the ERS represents a well traceable unit with lower seismic velocities, represented by lower amplitudes at the transition from the more porous sandstone to the conglomeratic but more dense Havel Subgroup in Fig. 7. Due to the low thickness of the ERS, the true thickness distribution could not be resolved from the seismic data directly. Therefore, we used the analysis of Bauer et al. (2020) to constrain its

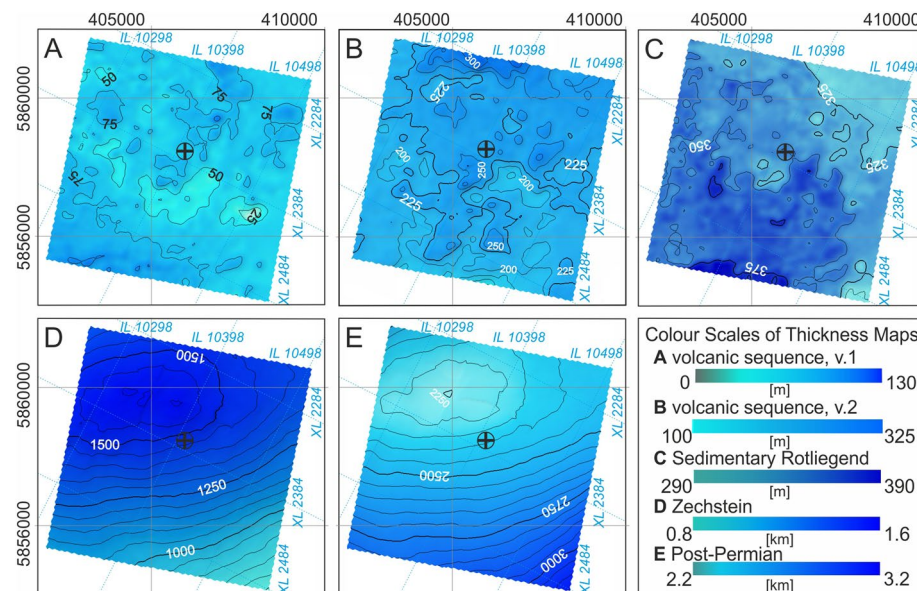


Fig. 8 Thickness maps determined from the 3D seismic data in Groß-Schönebeck (contour lines are given in meters; see text for detail). Two alternative interpretations of the Permo-Carboniferous volcanic succession are given, following the reflection found at the formerly hypothesized thickness of ca. 70 m (A) and the interpretation of the here introduced C1 reflector (B). C Sedimentary Rotliegend, D Zechstein, E Post-Permian succession. The cross marks the Groß Schönebeck drill site (E GrSk 3/90)

thickness better. In their approach, signal attributes are calculated along the ERS horizon using the continuous Morlet wavelet transform, based on a short mother wavelet to allow for the temporal resolution of the relatively short reflection signals to be analysed. The derived signal attributes were classified with a machine learning method. Subsequent modelling of the classification results provided estimates of layer thickness variations. Based on the seismic-well tie (Fig. 5), we picked the expected top and base of the ERS from the seismic data. Due to the thickness range, which is close to the seismic resolution for the corresponding depth, the mapped reflectors will not give a precise position of the depth interval of this lithological unit except for the wellsite locations, where we have direct information. Especially in the NW part of the volume, the top of ERS is hard to follow. To implement the results of the seismic facies analysis (Bauer et al. 2020) in the geological interpretation, we construct a theoretical medium positioning of the ERS (using the average depth of the mapped seismic reflectors of top ERS and base ERS) first. Then, trend maps of the thickness distribution from Bauer et al. (2020) together with the picked horizons and the borehole data were used to model a more representative thickness distribution of the ERS within the seismic volume.

Another reflector in the sedimentary Rotliegend is picked as *R3* reflector. It is interpreted as the top of the more sandy deposits of the Dethlingen Formation and may correlate to near of the base of Eldena (Fig. 2). The silty to clayey deposits of the Hannover Formation and uppermost Dethlingen Formation above the *R3* show often horizontal and less pronounced reflectors (Fig. 7).

Faults within the sedimentary Rotliegend are not traceable along several seismic lines. There are some indications for possibly subseismic faults in certain lines but they vanish on a very small scale, i.e., between two lines (< 30 m). Attribute analyses for the base of ERS and other horizons (like *R3* or *R6*) do not show any distinct fault pattern.

The sedimentary Rotliegend shows a smooth trend of lower depths in the northeast (about 4095 m) compared to the southwest (around 4185 m). The total thickness from the base of the Havel Subgroup (*R6*) to the base of the Zechstein succession (*Z3*) is increasing from NE to SW from about 300 to close to 400 m in the southern margin of the seismic volume with a mean thickness of 345 m (Fig. 8B).

The Zechstein deposits represent a succession of rocks with different density and sonic velocity, for instance of salt and anhydrite or salt and limestone. The resulting strong impedance contrasts are providing strong and distinct seismic reflectors in this formation. Due to the basin-wide cyclicity of the Zechstein deposits, these seismic markers are also traceable basin-wide on seismic sections. The base of Zechstein (*Z3*, Figs. 5, 6, 7) is seismically very well developed, because the anhydrite–mudstone transition from Zechstein to the Upper Rotliegend has a strong acoustic impedance contrast. It is located at a depth of ca. 3750–3800 m. In the E GrSk 3/90 borehole, the base of the Zechstein succession (the Werra Formation) consists of a 30-cm thick black mudstone (far below seismic resolution), representing the “Kupferschiefer”, 5 m of limestones and marlstones, and 67 m of anhydrite (intercalated with anhydritic halite). Above the Werra Formation, representing the first Zechstein cycle, the basal Staßfurt Formation (2nd Zechstein cycle) is composed of limestone (ca. 5.5 m thick) and anhydrite (ca. 2.5 m thick) which is overlain by more than 1115 m of halite, followed by 100 m of sylvine and ca. 1 m of anhydrite. The *Z1* reflector corresponds to

the transition of the Staßfurt salt to the underlying anhydrite (Fig. 5). The 3rd Zechstein cycle is represented by the Leine Formation. At the base, a couple of meters of dolomitic mudstones are present, followed by 45 m of anhydrite and 150 m of halite with an intercalation of 6 m thick clayey anhydrite. The impedance contrasts of the anhydrite of the Leine Formation and the rock salt of the Staßfurt formation cause another strong reflector (X3 or the so called “Z3 stringer” for the third Zechstein evaporation cycle (Table 2). The Aller and Ohre Formations represent the youngest two cycles of the Zechstein succession in Groß Schönebeck. Above a few meters of clayey and anhydritic sediments, salt rocks are present: ca. 50 m and 12 m in the Aller Formation and the Ohre Formation, respectively. The mapped X1 reflector corresponds to the anhydrite/rock salt succession near the top of the Zechstein. Figure 8C shows the thickness distribution of the Zechstein deposits that clearly outlines the anticlinal structure underneath Groß Schönebeck.

At the top of the anticlinal structure, a pronounced graben-like structure is present in the X3 horizon. The main faults are located ca. 1 km north of the E GrSk 3/90 borehole and is NW–SE oriented (Fig. 9A, B), showing an offset of up to ca. 30 m. This feature is one to more than two kilometres in length and exhibits a complex and circular fracture pattern at its SE margin. Because this pattern could not be mapped seismically in the overburden it is interpreted as an internal anhydritic and compact

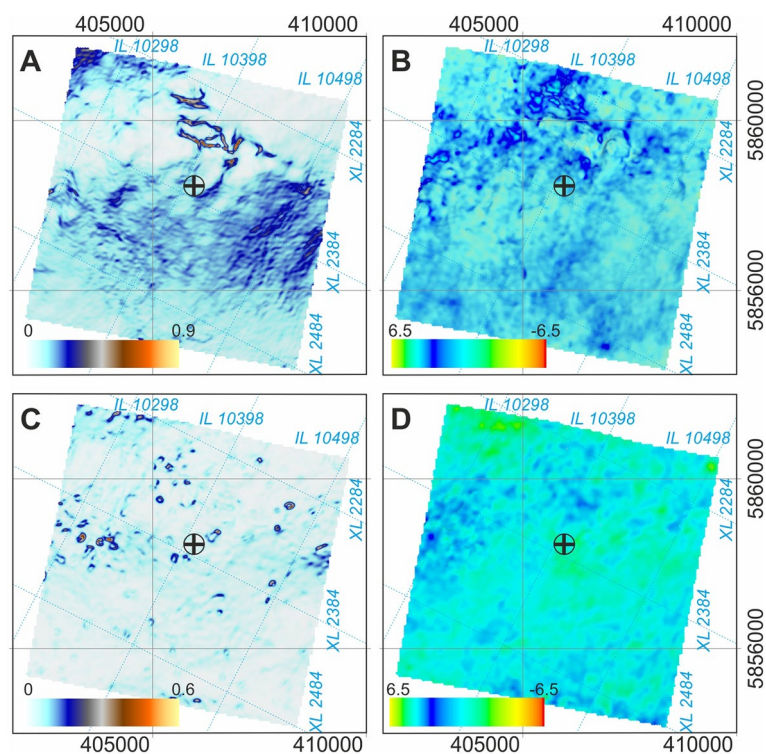


Fig. 9 Seismic attribute analysis applied for fault detection at the top (X3 horizon) and base (Z3 horizon) of Zechstein. Left column: variance along interpreted horizons based on CRS volume in time (A X3, C Z3). Right column: maximum amplitude based on CRS volume in depth (B X3, D Z3). The graben-like structure within the Leine anhydrite (X3, A, B) is clearly visible, while fault signatures are nearly absent at the base of the Zechstein (Z3, C, D). The cross marks the Groß Schönebeck drill site (E GrSk 3/90)

Zechstein stringer, overflow by rock salt that is more mobile. At the base of Zechstein (Z3), no basal faults are visible in the seismic volume (Fig. 9C, D).

Post-Permian

A number of reflectors show a continuous distribution pattern in the post-Permian succession. Most prominent are the S1 and S2 reflectors, the M1 and M2 reflectors, and the L2 and B2 reflectors (Fig. 5). In the seismic volume, those reflectors are very well developed in the southern area of the survey. They are less distinct north of the GrSk drillsite. Here, different effects are assumed to be responsible for this loss in quality of the seismic signal: the fracture zone indicated by the broken X3 stringer at the top of the anticlinal structure may extend toward the overburden and account for a scattering and damping of the seismic signal. The graben-like structure, clearly visible in the uppermost Zechstein, is not very distinct in the post-Permian succession. While the geometry of the fault pattern in the X1 horizon shows some similarity to the faults visible in the X3 horizon, the fault offset decreases and is no longer traceable in the M3 horizon. The less developed continuity of the seismic reflection horizons in the northern part of the study area, clearly visible in the CRS PreSDM volume, may reflect a fault system related to the deeper Zechstein salt pillow evolution, but not resolved in the 3D seismic data. The local sharply limited small-scale thickness variations north of the E GrSk 3/90 borehole shown in the compiled thickness maps (Fig. 10A–C) show the impact of these possible faults.

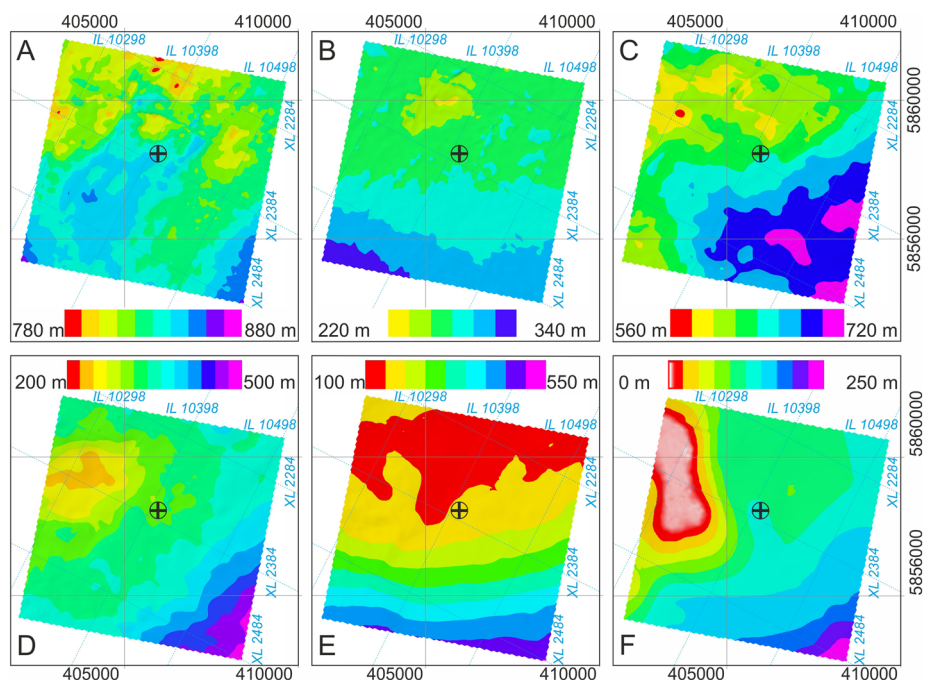


Fig. 10 Mesozoic and Tertiary thickness maps. **A** Buntsandstein (M3–X1), **B** Muschelkalk (M1–M3), **C** Keuper (L4–M1), **D** Jurassic (BLC–L4), **E** Cretaceous (based on Stackebrandt and Manhenke (2010) and the mapped BLC horizon), **F** Tertiary (mainly based on Stackebrandt and Manhenke (2010), combined with borehole data). The cross marks the location of the E GrSk 3/90 borehole

The general thickness distribution of the Mesozoic and Cenozoic sediments allows an interpretation of the salt pillow evolution. The Buntsandstein thickness shows a mean of 825 m within a variability of 780–880 m. Its distribution seems to be unrelated to the later salt structure (Fig. 10A). Only in the south-eastern and south-western corner of the study area, slightly enhanced thicknesses may indicate a first initiation of the salt structure development. The thickness of the Muschelkalk (Fig. 10B) shows a more generalized distribution pattern with larger thicknesses in the south and decreasing thicknesses toward the top of the anticlinal structure. The Muschelkalk thickness shows thereby a maximum variation (difference) of up to 120 m in the study area. An intense evolution of the salt structure is documented by the Upper Triassic (Keuper) sedimentary thickness distribution (Fig. 10C). The development of salt rim depression zones, where salt migrates toward the anticlinal structure, allows the sedimentation of greater sediment thicknesses, while the sedimentary thickness is reduced on top of the salt structure. This trend continues for the Jurassic and Cretaceous sediment thicknesses (Fig. 10D, E), indicated by the slightly increasing variation of the sedimentary thickness for the both units. The Tertiary sediment thickness is affected by the salt pillow topography and by the Quaternary occurred glacial overprint, resulting in the erosion of Tertiary sediments (incision trough, Fig. 10F).

Reservoir model

The previously described structural model provides the framework for a new Rotliegend reservoir model for further site development. The model comprises the Permo-Carboniferous volcanic rock section and the sedimentary Rotliegend. The geological modelling of the involved structural units and facies types represents the first step of the model construction. In a second step, we parameterized the respective units according to the available borehole and laboratory data.

Determination of parameters for facies modelling

Permo-Carboniferous volcanic rocks

The sequence encountered in the E GrSk 3/90 borehole consists of several layered lava beds and tuffs showing a single bed thickness of one to over three meter (based on core and microresistivity borehole image analysis, Fig. 11). Whereas the top of the volcanic sequence is well preserved by cores showing the transition to the conglomeratic deposits of the Havel Formation, the base of the volcanic sequence and hence its thickness is not proven by the available data. The volcanic rocks encountered in the E GrSk 3/90 borehole are of andesitic composition and show only subordinate fracturing. The rock core exhibits an amygdaloidal structure with variable crystal sizes. According to the observed effusive bed thicknesses, the unit was parameterized layerwise with a vertical resolution of about 2–3 m. Where volcanic bed boundaries could be observed in the borehole image log, they were picked, indicating an N to NNW oriented mean flow direction of the andesitic lava (330°). The thickness of a single volcanic layer amounts to about 30 cm for a tuff layer to about 7 m for an andesitic lava bed. Lavas do clearly dominate over pyroclastic deposits and the mean dip of the surfaces amounts to 15° (showing a range of 5 to 60°). Therefore, it is expected that the Groß Schönebeck site is located in a near-medial to a near central proximal distance to the volcanic vents according to Bogie and

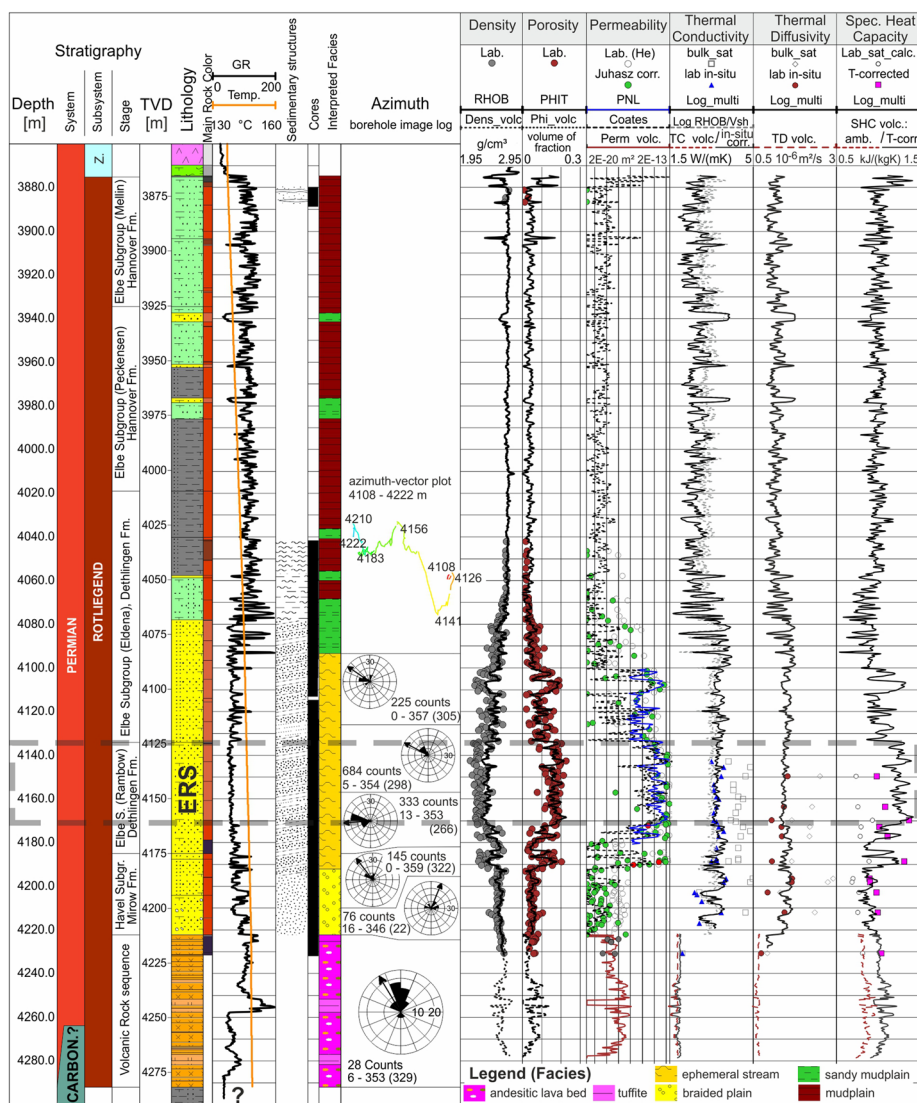


Fig. 11 Core and log interpretation (E GrSk 3/90). Structural data from microresistivity borehole imaging (not shown in panel), the sedimentary section is based on Holl et al. (2005). The Elbe reservoir sandstone (ERS) is highlighted by the thick grey stippled line. CARBON.: Carboniferous; density: Lab.—laboratory determined bulk density, RHOB—bulk density from logging, Dens_vo—density of volcanic rocks; porosity: Lab.—porosity determined on core samples, PHIT—total porosity from well-log interpretation, Phi_vo—porosity estimated from sonic log; permeability: Lab.(He)—routine gas permeabilities, uncorrected, Juhasz corr.—in-situ corrected Lab.(He) perms: green dots, PNL—permeability from pulsed-neutron logging, Coates—permeability using the Coates equation, Perm_vo.—permeability of volcanic rock, red dots—brine-permeabilities measured under in-situ conditions; thermal conductivity/thermal diffusivity: bulk_sat—measured under ambient saturated conditions, lab in-situ—corrected for in-situ p/T conditions; Log_multi—log-derived thermal properties of sedimentary (clastic) rocks, TC_vo—ambient and in-situ corrected thermal conductivity of volcanic rock, TD_vo.—in-situ thermal diffusivity of volcanic rocks; Specific heat capacity: Lab_sat_calc.—calculated (ambient conditions), T-corrected—temperature corrected values, SHC_vo—ambient and temperature-corrected specific heat capacity of volcanic rock

Mackenzie (1998) and that the general volcanic succession will not change fundamentally within the modelled seismic volume. However, the overall thickness of the sequence is questionable, and therefore, the composition and structuring of the sequence beyond well control is provisional. Following the hitherto assumptions (see “Permian” section

above and, e.g., Holl et al. 2005), the sequence may show a thickness of about 70 m or more than 200 m. We set up two models, one considering a thickness of 70 m (model A, shown in the following) and one considering a thickness of 200 m (model B, see discussion) based on the weak seismic reflector observed at a depth level of about 4.4 km.

Sedimentary Rotliegend

For reservoir simulation, four different sedimentary facies types were considered (Fig. 11, Table 4). Most of the coarse-grained bed-load dominated and conglomeratic deposits of the Havel Formation are interpreted as multi-storeyed channel sediments of a *braided plain fluvial* system with a paleocurrent direction toward NNE (Holl et al. 2005). To investigate the geometrical setting of this fluvial system, we determined the mean (s_m) and deviation (s_d) of cross-bed thickness from the borehole image log of the E GrSk 3/90 borehole (0.59 m and 0.27 m, respectively). Following Bridge and Tye (2000), the mean dune height (h_m) could be estimated with

$$h_m = 2.22 \cdot \left(\frac{s_m}{1.8} \right) \quad (6)$$

if s_m/s_d equals “approximately 0.88 ± 0.3 ”. A generous interpretation of this criteria, (s_m/s_d accounts to 0.5), will allow the calculation of h_m and the mean dune depth d_m according to Allen (1970, cited in Bridge and Tye 2000) with

$$d_m = 11.6 \cdot h_m^{0.84} \quad (7)$$

In our case, this may reflect a paleochannel depth of about 9 m (see Bridge and Tye 2000; Leclair and Bridge 2001) and correlate to a channel belt width of about 3500 m according to empirical correlations given by Bridge and Mackey (1993), to estimate the possible minimum (min) and maximum (max) channel-belt width (cbw):

$$cbw_{min} = 59.9 \cdot d_m^{1.8} \quad (8)$$

$$cbw_{max} = 192 \cdot d_m^{1.37} \quad (9)$$

As our study relies on data from one borehole (E GrSk 3/90) only and the used equations cover a huge spectrum of very different fluvial systems (see, e.g., Gibling 2006) and have in general considerable large uncertainties for estimating the width, thickness and overall geometry of fluvial channel bodies buried under the surface, the deduced geometrical parameter given in Table 4 may represent a rough estimation of the principal architecture.

The second facies element represents the *ephemeral stream floodplain* environment identified by Holl et al. (2005) for the Dethlingen Formation. As described by the authors, the fine- to coarse-grained sandstones are amalgamated in character and show fining-upward trends to the top of the formation, representing proximal to distal fluvial facies. Transport direction is toward W and NW ($265\text{--}305^\circ$). Within the lower part of the Dethlingen Formation the ERS is developed and shows small-to-large-scale cross-bedded and low-angle cross-bedded sandstones as well as horizontally laminated sands (Fig. 11). The sediments are interpreted as fluvial reworked

Table 4 Input data and ranges for facies simulation

Unit	Stratigraphy	Modelled reference facies	Depth range (m) (E GrSk 3/90)	Background facies	N/G ratio ^a (dec)	Main lithology	Channel geometry: ranges, mean value in brackets				
							Orientation ^b (°)	Amplitude (km)	Wavelength (km)	Width (km)	Thickness ^b (m)
7	Upper Hannover Fm. (Mellin)	Sandy mudflat	3875–3901	Mudflat playa	0.02	Mudstone	Like sandy mudflat in unit 5				
6	Hannover Fm. (Mellin-Peckensen)	Sandy mudflat	3901–3941	Mudflat playa	0.1	Mudstone, and siltstone, and some sandstone	Like sandy mudflat in unit 5				
5	Dethlingen to Hannover Fm. (Peckensen-Eldena)	Sandy mudflat	3941–4084	Mudflat	0.4	Siltstone, fine-grained sandstone	275–360 (300)	0.8–2.5 (1.5)	1.0–5.0 (2.5)	0.005–0.4 (0.06)	0.2–8.0 (2.0)
4	Dethlingen Fm. (Eldena)	Epheremal stream flood-plain	4084–4134	Sandy mudflat	0.85	Siltstone, fine-grained sandstone	200–360 (290)	0.6–2.5 (1.7)	2.0–8.0 (4.0)	0.7–3.3 (2.1)	4.0–8.0 (6.0)
3	Dethlingen Fm. (Rambow, ERS)	Epheremal stream flood-plain	4134–4185	Sandy mudflat	0.99	Fine- to coarse-grained siltstone	225–340 (290)				
2	Mirow Fm. (Havel subgroup)	Braided river	4185–4222	Sandy mudflat	0.8	Coarse-grained sandstone and conglomerate	290 (-70)–90 (345)	0.6–2.5 (1.7)	2.0–8.0 (4.0)	2.5–4.5 (3.5)	8.0–12.0 (9.0)
1	Permo-Carboniferous	Tuffite, massive andesite	4222–4292	None	0.85	Amygdaloidal andesitic rocks	290 (-70)–45 (355)	–	–	Several km	0.3–7.0 (2)

The N/G ratio refers to the global net-to-gross ratio of sandy (porous) to non-porous rocks, in *italic*: corresponding parameters chosen after Gibling (2006)

^a Based on the GR log of the E GrSk 3/90 borehole

^b Estimated using the image log of E GrSk 3/90

aeolian deposits. The estimation of the geometrical architecture of the stream floodplain based on borehole interpretation shown in Table 4 is based on a mean bed thickness and thickness deviation of 0.32 m and 0.2 m. Bar thicknesses, estimated from log data, showed a range of 4–8 m, giving some support for the interpretation. Based on the higher resolution of the DAS–VSP seismic data, Martuganova et al. (2022) could map a 20–30 m thick horizon within the Dethlingen Formation, which they interpreted as a higher porous sandy reservoir section, possibly representing the seismic visible part of a stacked channel architecture. However, internal channel structures are not resolved by the data that is itself limited to the near-borehole area. We, therefore, use this information as a depth-related trend volume to guide the petrophysical modelling of the ERS, demanding for higher porosities in this zone (see also next section).

The sandy mudflat and mudflat facies types of the Dethlingen and Hannover Formations were represented by finer siliciclastics, indicating the transition to the Zechstein transgression. Borehole image logs are not available for this section. For the *sandy mudflat* environment, siltstone and fine-grained sandstones are present which are interpreted as deposits of sporadic higher current velocities in channel-like structures, assuming the architectural parameters presented in Table 4 (inspired the range for crevasse channels given by Gibling 2006). The *mudflat facies* finally consists of mudstones of the playa environment without channels.

Petrophysical modelling

Permo-Carboniferous volcanic rocks

The petrophysical properties of this sequence was evaluated based on the available laboratory measurements of density, porosity, permeability, and log analysis (Table 2, Fig. 11). Because only GR and Sonic logs and today only limited core material are available for the lowermost section of the borehole, the core-log analysis of this section represents a first order estimate. The sonic-derived porosity will most likely overestimate the connected porosity needed for the permeability estimation according to Siratovich et al. (2014). However, the resulting permeability (brown “Perm volc.” line in Fig. 11) shows a quite reasonable match with the few values of laboratory-determined permeabilities. Based on the estimated log permeability, its anisotropy was calculated as the ratio between the harmonic and the arithmetic averages for 2-m depth intervals (see Table 5).

In terms of petrophysical properties, the tuffite and the andesitic lava beds most likely exhibit some differences (Fig. 11) which could not be evaluated further based on the available data quality. Total porosity (PHIT) of the igneous section was modelled facies-dependent for the modelled layers based on the input data given in Table 5. As a next step, bulk density (RHOB), effective porosity of interconnected pores (PHIGE), and fluid permeability (PERM) were simulated considering the PHIT distribution (using the collocated co-Kriging function, see Table 5). The thermal conductivity (TC) of the succession was estimated by the approach of García et al. (1989) using the attributed PHIT and BD distributions. A pT-correction was applied by cross correlation of the ambient and corrected TC values from the log interpretation [$TC(pT\text{-corrected}) = 0.8464 * TC + 0.3707$]. The specific heat capacity (SHC) was calculated using the PHIT and RHOB distributions

Table 5 Input parameter used for petrophysical modelling of the volcanic rock section

	Tuffitic layers		Andesitic lava beds		
	Model parameter	Well log data	Model parameter	Well log data	Core data
bed thickness (m)	0.3–2.9 (1.4)	Interpreted from E GrSk 3/90 and Gt GrSk 4/05	0.4–7.0 (2.2)	Interpreted from E GrSk 3/90 and Gt GrSk 4/05	
PHIT (dec)	0–0.13 (0.05 ± 0.02)	0–0.13 (0.03 ± 0.03) [31]	0–0.11 (0.06 ± 0.02)	0–0.11 (0.04 ± 0.02) [195]	–
PHIG ^b (dec)	0–0.06 (0.02 ± 0.01)	Not evaluated	0–0.08 (0.04 ± 0.01)	Not evaluated	0.03–0.06 (0.05 ± 0.01) [11]
BD ^c (kg/m ³)	2420–2890 (2660 ± 120)	2422–2878 (2682 ± 84) [31]	2460–2830 (2640 ± 103)	2460–2763 (2623 ± 60) [195]	2580–2655 (2632 ± 28) [11]
PERM (m ²)	0–8.9E–17 (9.90E–18)	1.77E–21 to 8.5E–16 (1.75E–19; GSD: 66, ranging from 2.66E–21 to 1.15E–17) ^a [31]	0–5.9E–17 (9.90E–18)	1.77E–21 to 6.11E–17 (4.83E–18; GSD: 17.4, ranging from 1.11E–18 to 2.09E–17) ^a [195]	0–1.38E–17 (4.9E–19; GSD: 17.4, ranging from 2.82E–20 to 8.52E–18) ^a [10]
TC (Wm ^{–1} K ^{–1})	1.4–2.1 (1.9 ± 0.1)	1.5–1.9 (1.9 ± 0.1) [31]	1.6–2.1 (1.9 ± 0.1)	1.6–1.9 (1.9 ± 0.1) [195]	2.1 [1]
TD (10 ^{–6} m ² s ^{–1})	0.50–0.82 (0.69 ± 0.03)	0.58–0.78 (0.75 ± 0.05) [31]	0.55–0.80 (0.69 ± 0.03)	0.61–0.78 (0.73 ± 0.04) [195]	0.83 [1]
SHC (Jkg ^{–1} K ^{–1})	884–1195 (1021 ± 66)	888–1190 (981 ± 75) [31]	903–1154 (1030 ± 60)	920–1153 (1015 ± 47) [195]	976 [1]
Variogram input ^d	2000/1500/2, 330	–	2000/1500/3, 330	–	–

Given is the range and mean (in brackets) chosen for the modelling and the supporting well-log and core data (if available) with the respective standard deviation and the number of observations (in square brackets)

^a Geometric mean with geometric standard deviation factor (GSD)

^b Collocated co-Kriging with total porosity (PHIT) using a correlation coefficient of 0.8

^c Collocated co-Kriging with total porosity (PHIT) using a correlation coefficient of –0.8

^d Input for a spherical variogram (given: major/minor/vertical [m], azimuth [°]). If not specified otherwise, all data refer to the E GrSk 3/90 borehole, laboratory thermal data are corrected to in-situ conditions, see text

following the approach of Heap et al. (2020). Cross-correlation of T-corrected and ambient heat capacity from log analysis yield a simple correction function to correct the heat capacity for in-situ conditions [SHC(T-corrected) = 1.237 * SHC – 0.01527]. Finally, the in-situ thermal diffusivity (TD) of the igneous rocks was derived from the determined properties with TD = [TC (pT-corrected)]/[SHC (T-corrected) * RHOB].

Sedimentary Rotliegend

For the evaluation of petrophysical properties, we could rely on the extensive data set of the E GrSk 3/90 borehole (Table 2, Fig. 11). Permeability is shown from single borehole logging (via pulsed-neutron logging, PNL) and based on implementation of the Coates equation. The constants for the Coates relation are fitted manually, resulting in values of 750, 6, and 1.4, for *a*, *b*, and *c*, respectively. The derived Coates permeability log shows a general agreement with the permeability estimated by the PNL, but in general a better agreement with the in-situ corrected laboratory-derived permeability data (“Juhasz corr.”, Fig. 11). Three permeability measurements conducted under in-situ conditions (Trautwein 2005) are plotted in Fig. 11 (red dots), which seem to confirm the correction

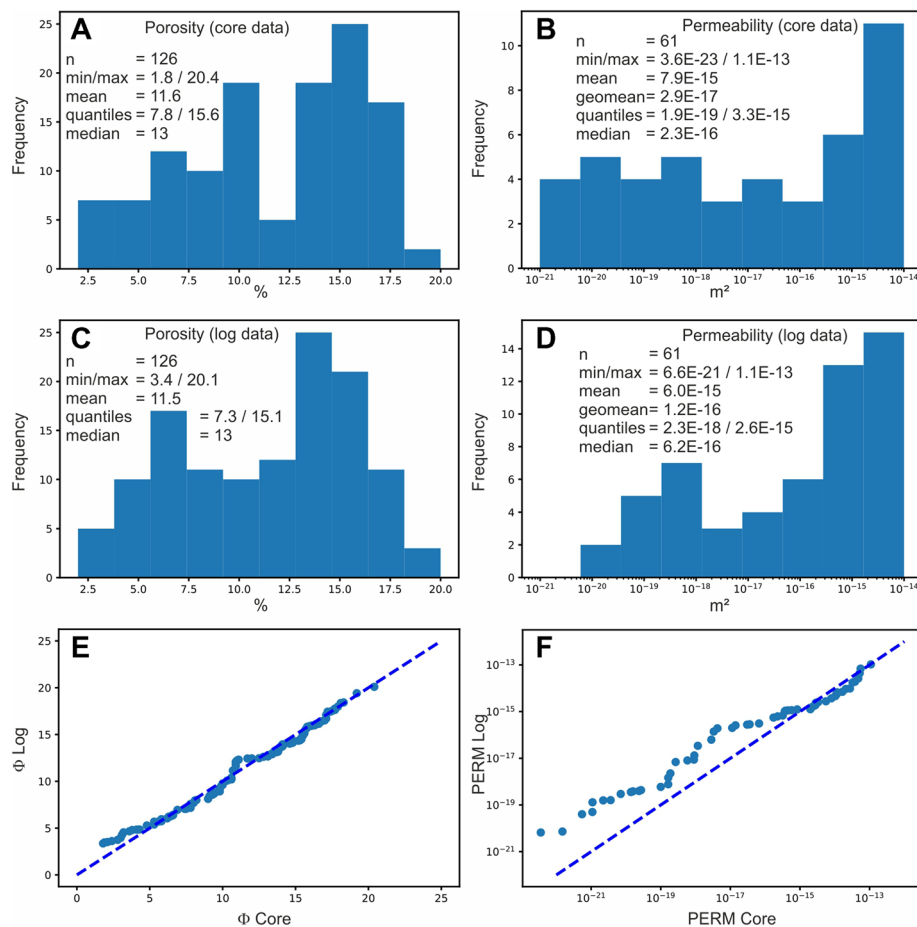


Fig. 12 Histograms (a–d) and quantile–quantile plots (e, f) of total porosity (in %) and permeability (in mD) for core data (a, b) and corresponding log-based data (c, d) for the stream floodplain facies of the EBS (E GrSk 3/90)

approach. The comparison of core and log data (Fig. 12) shows roughly a similar distribution, the paired quantile–quantile plot of the effective permeability shows, however, that the log-derived permeability of permeabilities less than $10\text{E}^{-15} \text{ m}^2$ ($< 1 \text{ mD}$) deviates from the corrected core data, providing slightly higher permeabilities.

Anisotropy (calculated as the ratio between the harmonic and the arithmetic averages of log-derived permeability) ranges from 0.2 to 0.6 for a grid size of 1 m, depending on the respective facies (Table 6). TC, TD and SHC were determined from log analysis according to Fuchs et al. (2015). TC was estimated on the combination of the neutron-porosity (NPHI) log, the sonic log, and the gamma ray (Vshale) log (Log_multi, Fig. 11) as well using the bulk density (RHOB) and Vshale logs only (Log RHOB/Vsh, Fig. 11). TD (log_multi) is using RHOB, NPHI and Vshale log, while the SHC was evaluated using RHOB, NPHI, and Vshale as input logs (the data and the calculation is also provided in the data publication to this manuscript). In Fig. 11, the log-derived thermal properties are plotted together with the laboratory measurements that were corrected to in-situ p/T-conditions. For TC, by applying the

Table 6 Input parameter used for petrophysical modelling of the sedimentary Rotliegend

	Braided plain fluvial			Ephemeral stream floodplain			Sandy mudflat			Mudflat playa		
	Model	Well log data	Core data	Model	Well log data	Core data	Model	Well log data	Core data	Model	Well log data	Core data
PHIT (dec)	0–0.16 (0.05)	0.01–0.08 (0.05 ± 0.01) [120]	0.01–0.08 (0.04 ± 0.01) [46]	0–0.21 (0.11)	0.03–0.20 (0.11 ± 0.05) [395]	0.02–0.20 (0.12 ± 0.05) [135]	0–0.17 (0.05)	0.01–0.07 (0.03 ± 0.01) [189]	0.01–0.10 (0.04 ± 0.02) [27]	0–0.18 (0.04)	0–0.16 (0.04 ± 0.02) [684]	0.01–0.03 (0.02 ± 0.01) [11]
PHI _{GE} ^b (dec)	0–0.05 (0.0)	0–0.03 (0.01 ± 0.01) [120]	–	0–0.18 (0.08)	0–0.18 (0.05 ± 0.04) [395]	–	0–0.11 (0.03)	0–0.05 (0.01 ± 0.01) [189]	–	0–0.01 (0.0)	< 0.01	–
BD ^c (kg/m ³)	2510–2690 (2590)	2507–2688 (2589 ± 30) [120]	2450–2680 (2567 ± 46) [46]	2280–2690 (2450)	2283–2695 (2450 ± 83) [395]	2110–2640 (2349 ± 128) [135]	2510–2740 (2660)	2513–2740 (2653 ± 55) [189]	2380–2700 (2569 ± 78) [27]	2630–2750 (2710)	2343–2813 (2706 ± 38) [686]	2660–2730 (2685 ± 17) [11]
V _{shale} (dec)	0.1–0.6 (0.2)	0.08–0.54 (0.28 ± 0.13) [120]	–	0.01–0.5 (0.1)	0.01–0.52 (0.11 ± 0.09) [395]	–	0.01–0.7 (0.3)	0.01–1.0 (0.35 ± 0.26) [189]	–	0.01–0.8 (0.6)	0.02–0.79 (0.48 ± 0.13) [686]	–
TC (Wm ⁻¹ K ⁻¹)	2.0–4.1 (3.7 ± 0.2)	2.8–3.9 (3.5 ± 0.3) [109]	2.6–3.9 (3.2 ± 0.6) [7]	2.0–4.2 (3.6 ± 0.2)	2.9–4.1 (3.6 ± 0.2) [395]	3.3–3.8 (3.5 ± 0.2) [18]	2.0–4.1 (3.2 ± 0.3)	1.7–4.1 (3.2 ± 0.6) [189]	–	1.6–3.9 (2.2 ± 0.2)	1.9–3.9 (2.7 ± 0.3) [686]	–
TD (10 ⁶ m ² s ⁻¹)	0.77–1.92 (1.67 ± 0.08)	1.32–1.75 (1.58 ± 0.12) [120]	1.02–1.74 (1.50 ± 0.34) [4]	0.78–1.91 (1.56 ± 0.15)	1.36–1.84 (1.56 ± 0.10) [395]	1.14–1.61 (1.38 ± 0.19) [6]	0.77–1.86 (1.49 ± 0.10)	0.89–1.83 (1.48 ± 0.24) [189]	–	0.72–1.78 (1.04 ± 0.07)	0.92–1.79 (1.25 ± 0.14) [686]	–
SHC (Jkg ⁻¹ K ⁻¹)	750–1314 (846 ± 37)	736–961 (870 ± 52) [120]	821–922 (871 ± 51) [4]	758–1314 (939 ± 88)	775–1384 (1089 ± 153) [395]	878–1117 (977 ± 95) [6]	731–1314 (816 ± 36)	534–1080 (869 ± 102) [189]	–	718–1314 (817 ± 60)	684–1350 (965 ± 81) [686]	–

p-correction formula of Emirov et al. (2017) and the T-correction formula of Somerton (1992), for SHC by applying the T correction given by Waples and Waples (2004), and for estimating in-situ TD this properties is calculated based on the in-situ TC, the temperature corrected SHC, and the respective laboratory-derived bulk density. The log-derived values and the laboratory values show a very good agreement, allowing parameterizing the sedimentary Rotliegend succession in a consistent manner.

To do so, we first addressed the total porosity (PHIT). Depending on the respective facies, the PHIT distribution was modelled using the geostatistical input provided in Table 6. For the ERS, the seismic facies analysis of Bauer et al. (2020) and the DAS-VSP analysis of Martuganova et al. (2022; for the near-borehole area only) were used as additional trend information for the general probability of higher porosities in the sandy reservoir section. PHIGE of this unit was modelled in relation to PHIT using the collocated co-kriging algorithm of Petrel (Table 6). For a representative and consistent parameterization with permeability (PERM) and thermal properties, bulk density (RHOB) of the rocks and the Vshale content were assigned to the grid cells. They were simulated based on the distribution of PHIT (for RHOB) and of PHIGE (for Vshale) using the input parameters specified in Table 6. PERM was calculated on PHIT (Table 6) and in-situ TC and TD were estimated using the RHOB and Vshale distributions based on the formulas [A55] and [B55] of Fuchs et al. (2015). Using the log interpretation, the RHOB and Vshale-based TD was correlated with the NPHI, Vshale, and RHOB-based TD. The SHC of the sedimentary section was calculated using the estimated distributions of TC, TD, and RHOB according to $SHC = TC / (TD * RHOB)$, for details see data publication.

Figure 13 illustrates the facies-dependent parameterization of the geological model, addressing the mentioned petrophysical properties. In the vertical distribution of the modelled properties, the Permo-Carboniferous volcanic rock sequence (unit 1) at the model bottom shows clearly a layered character, low porosities and different thermal properties than the overlying sedimentary units. The dense conglomeratic rocks of the Mirow Formation (unit 2) show similar bulk densities as the volcanic rocks, but show considerably different transient thermal properties compared to the adjacent model units (Fig. 13h, i). Unit 3 (Dethlingen Formation), containing the ERS, is most prominent by showing higher permeabilities compared to the surrounding units. The formations above unit 3 are characterized by fine-grained sediments of playa and mud-flat environments, resulting in higher shale content, lower specific heat capacities, and with overall much poorer reservoir properties (Fig. 13). Although the thickness of unit 3 is more or less constant along the section shown in Fig. 13, the parameter of the facies model provokes also some lateral and vertical variation in the property distribution. The lateral variation is also guided by the seismic facies analysis for the ERS, indicating areas of higher porosity or thickness of the ERS. Figure 14 shows the modelled thickness and the distribution of PHIT, Vshale, PERM, and TC, guided by the seismic facies analysis and the interpreted geophysical and laboratory data.

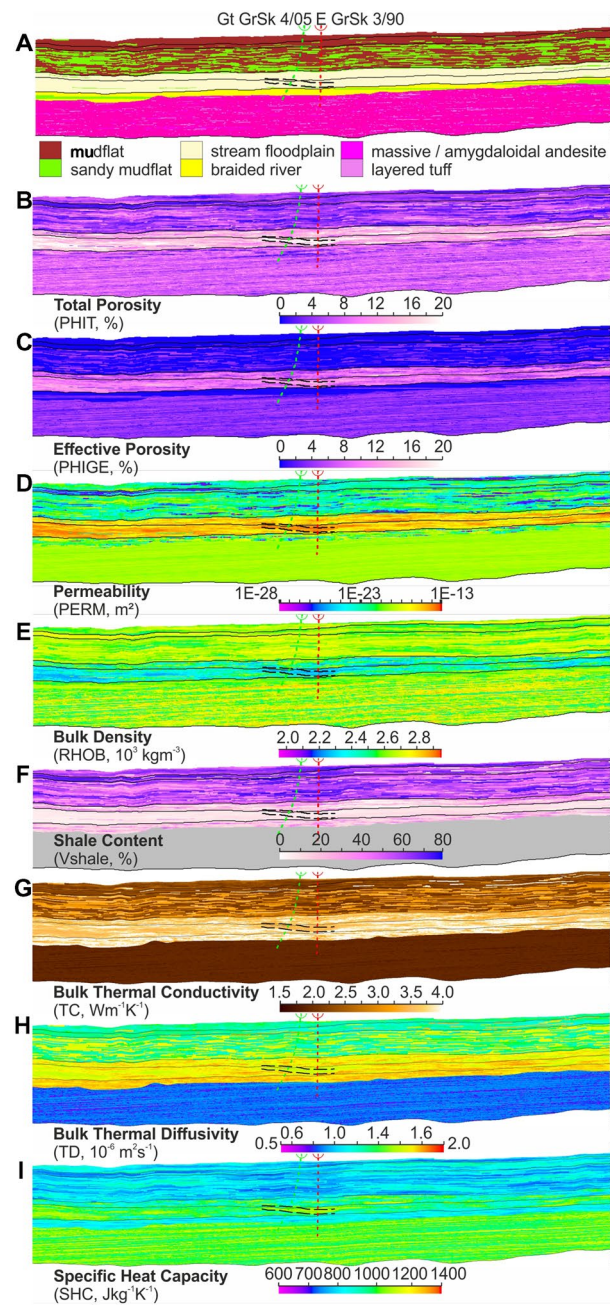


Fig. 13 Facies (a) and petrophysical parameterization (b–i), assuming a thickness of the volcanic sequence of about 200 m. Shown are 6.5 km long W–E cross sections covering the central part of the seismic survey in the depth range of 3800–4400 m, located approximately 75–200 m north to the Groß Schönebeck boreholes (views from the south). Exaggeration: approximately 1.5

Discussion

The new 3D seismic of the Groß Schönebeck area (Fig. 15) allows a more detailed interpretation of the geological structures of the subsurface and provides a solid framework for the site model building and its petrophysical parameterization.

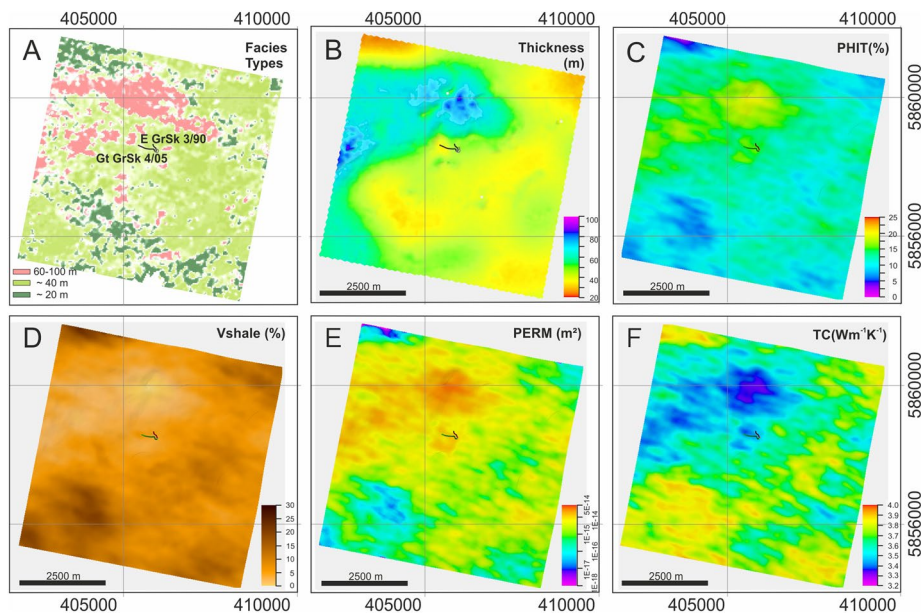


Fig. 14 Analysis of the Elbe reservoir sandstone (ERS) derived from reservoir and seismic modelling. **A** Seismic facies types in the EBS according to Bauer et al. (2020), **B** Thickness map of the EBS (unit 3 in the geological model). Average property maps of the EBS showing total porosity (PHIT, **C**), shale content (Vshale, **D**), permeability (mD, **E**), and thermal conductivity (TC, **F**). Superimposed are the borehole paths of the GrSk boreholes (black lines in panel centres)

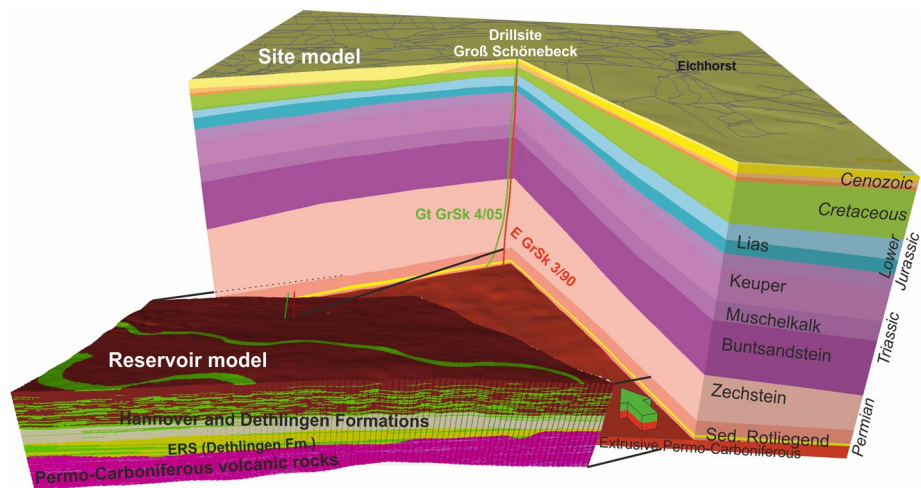


Fig. 15 Block visualizations of the new site and reservoir models of the Groß Schönebeck research platform, view from south. The size of the site model is 10 km × 10 km, the size of the reservoir model 6.5 km × 6.5 km

Structural information

The structural interpretation shows some very distinct and clear features, like the salt pillow distribution pictured by the pronounced Zechstein reflectors, and more ambiguous elements, such as the base and thickness of the Permo-Carboniferous volcanic sequence.

The top of the volcanic sequence is often well recognizable in seismic sections (Rieke et al. 2001) due to their contrast in the acoustic behaviour of the overlying clastic Rotliegend sediments. However, the base could most often not be deciphered in seismic data. Also for the Groß Schönebeck area, the base of the volcanic rocks could not be clearly correlated with a seismic event. The top of Carboniferous as interpreted for the E GrSk 3/90 well was based on the geophysical log interpretation for the lowermost logged section, postulating that the deepening of the E GrSk 3/90 well already drilled sedimentary rocks of Carboniferous age (Holl et al. 2005). At a first glance, the results of Regenspurig et al. (2016) seems to support this interpretation. They refer to geochemical analysis of drill cuttings from the Gt GrSk 04/05 well which would classify the volcanic rock as dacite or rhyodacite according to the TAS Diagram (Le Maitre 2002). These rock types could relate to the first (oldest) eruption stage in Brandenburg and would, therefore, support the interpretation that the sedimentary Carboniferous may be present close by. However, further analysis performed on core samples of the correspondent depth interval from the adjacent E GrSk 3/90 borehole classify the cored volcanic rock as andesite (Lotz 2004). Thus, they may represent the latest eruption stage instead. An explanation for this contradiction could result from a potential contamination of the drill cuttings of the Gt GrSk 4/05 well. Due to a large open-hole section, the finely grounded cuttings (not allowing to depict any rock fragments or structures) may be enriched with silica minerals (quartz) from the sedimentary overburden. There are further indications that the overall thickness of the volcanic sequence accounts for more than 70 m. Bauer et al. (2010) analysed seismic wide-angle data around the Groß Schönebeck site and modelled a reflector in a depth of about 4.7 km which is interpreted to correlate to the top of the Pre-Permian. Taking the uncertainty in depth conversion and the different seismic data types into account, this depth matches better to the lower C1 reflector (scenario B) with a depth of about 4.4 km than to the upper C1 reflector (scenario A) with a depth of about 4.2 km. This upper C1 horizon may represent an internal feature of the volcanic succession (intermediate sedimentary layer or tuffite) rather than the top of the (sedimentary) Carboniferous. Greater volcanic thicknesses were also expected by former studies. Benek et al. (1996) and Benek and Hoth (2004) assumed a thickness of 200–400 m for the study area, a range that is also in agreement with legacy exploration data of the former GDR estimating a thickness of about 250 m (Hoth and Huebscher 1986). The different thickness scenarios will have an impact on the further site development. Therefore, a proper seismic-well tie for the top of Carboniferous would be of high relevance. One way to access these data could be achieved by deepening of the E GrSk 3/90 well by coring. Even if Carboniferous rocks were encountered, their characterization would allow an optimized development of an EGS.

For the sedimentary Rotliegend, the 3D seismic provides evidence that faults with large offsets are apparently absent in the study area. Based on the analysis, the Rotliegend of the studied area does not show any segmentation into fault blocks. This is in contrast to the previous assumptions of a pronounced Rotliegend fault system in that area (e.g., Moeck et al. 2009). The supposed faults, interpreted on re-processed 2D seismic lines using complex attribute analysis, could not be confirmed by the 3D seismic volume. Thus, large and pronounced fault systems were not present in the data. Subseismic joints are, however, expected. Interpretation of microseismic events due to hydraulic

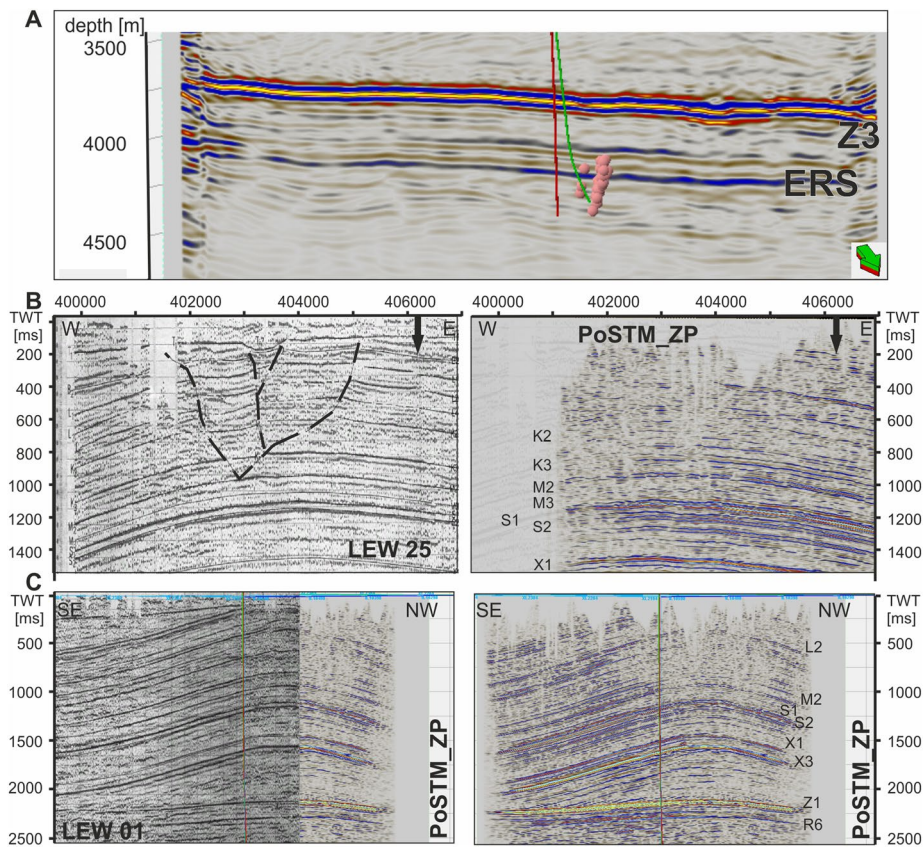


Fig. 16 Examples of the high-resolution imaging achieved by the 3D seismics (Krawczyk et al. 2019), targeting Permo-Carboniferous geothermal reservoirs in direct comparison with former investigations. **A** Shows the micro-seismic events registered during fluid injection (Kwiatek et al. 2010) superimposed on a cross section cut from the 3D seismics (Xline 2385, view from south), **B** and **C** show the 2D legacy lines LEW25 (view from south) and LEW 1 (view from northeast) on the left-hand side, respectively (courtesy Neptune Energy). For comparison, the corresponding sections cut from the new 3D seismics is shown on the right. The arrow marks the projected drill site of Groß Schönebeck. Stippled lines show former fault interpretations

stimulations (Kwiatek et al. 2010) do suffer from the challenges in accurate location of the events but give some ideas on the possible orientation of fault planes. The events, however, do not coincide with structures within the seismic volume (Fig. 16A). In this context it is of interest that Blöcher et al. (2018) assume the existence of a fault along the microseismic events, but they also state that they would expect seismic events for two previously interpreted faults nearby the stimulated area, which did not occur. In consequence, they questioned their existence. This interpretation, which is based on their numerical model of coupled thermal–hydraulic–mechanical processes for accessing the fault reactivation potential and its alteration during a waterfrac stimulation treatment, is in agreement with the results from the geological interpretation of the 3D seismic survey, where no distinct faults could be mapped.

Our study allows some further information on the timing and evolution of the salt pillow of Groß Schönebeck, which started in the Upper Buntsandstein and continues in the Cretaceous to Cenozoic. The mapped graben structure at the top of the anticline (related to the X3 horizon) are interpreted as internal Zechstein structures, resulting

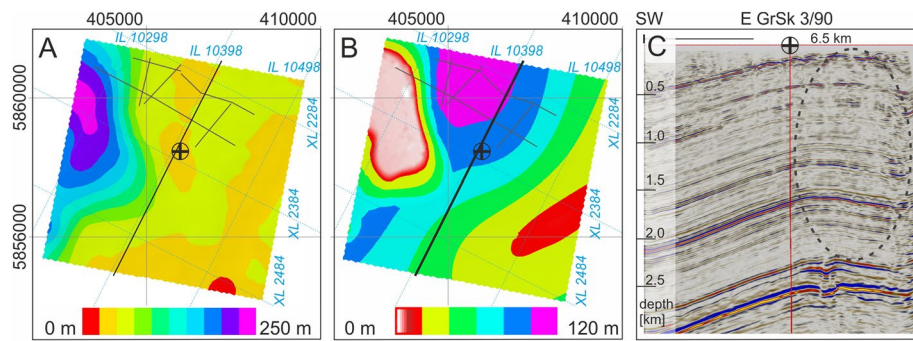


Fig. 17 Thickness maps of the Quaternary deposits (A) and of the Tertiary Rupelton (B) based on Stackebrandt and Manhenke (2010). Superimposed in grey lines are the mapped main faults in the upper Zechstein (this study) and the orientation of the seismic profile shown in C. C Seismic section of the pre-stack depth migration volume with CRS stack after depthing (profile D in Fig. 6) showing less continuity of seismic reflectors in the stippled area

from broken anhydritic layers which were passed by more ductile rock salt. A similar process is described by Strozyk et al. (2012) for the western Dutch offshore for the so-called Z3 stringer (corresponding to the anhydrite of the Leine formation, reflector X2 to X3). This interpretation is also supported by the fact, that the post-Permian reflectors do not show any distinct fault patterns in the 3D seismic. The uppermost reflector that could be tracked more or less completely in the volume is the Jurassic L2 reflector. The seismic to well-tie (Fig. 5) relies on several types of input data and is expected to represent a robust interpretation, especially for depths below 0.5–1 km. Comparing different time-to-depth conversions and former interpretations on legacy seismic data, this uppermost depth level shows often slightly different correlations for the seismic horizons. However, signal strength and resolution do not allow a detailed interpretation of the structural and internal layering of post Jurassic strata. Former interpretations based on one 2D seismic section reaching into the northwest of the 3D seismic area (e.g., LEW25/01, Figs. 1, 16B, C) show some discontinuous reflectors (courtesy of Neptune Energy). Due to the lower resolution of the 3D seismic at shallower depths (the survey was designed to study the Permo-Carboniferous targets) and the overall reduced seismic signal in that area, faults could not be tracked here. This may indicate a somehow distorted layering of the strata with offsets below the seismic resolution or just be related to a worse acoustic coupling due to higher thicknesses of younger sediments with low densities. From surface studies, Hardt et al. (2021) interpret Quaternary landforms to result from the interaction of glacial tectonics and halo tectonics. Their location corresponds to the area, where the deep fracture is assigned in the 3D seismic volume. Besides acoustic scattering triggered by a fracture system, significant changes in the near-surface geology may represent another factor affecting the quality of the seismic signal within the post-Permian. Figure 17 shows the thickness distribution of Quaternary sediments in the study area and the thickness of the Tertiary Rupelton according to Stackebrandt and Manhenke (2010). In the north-western part of the study area, a Quaternary incision trough cuts into the Tertiary Rupelton allowing the deposition of more than 200 m-thick unconsolidated Quaternary sediments, while the mean Quaternary sediment thickness in the remaining area

amounts to about 50–75 m (Fig. 17A). In the area of the incision trough, the seismic signal is less pronounced like for the northern part of the seismic volume. However, no deep fractures are observed in the Zechstein reflectors here. The Quaternary incision trough also reduces the thickness of the Tertiary Rupelton that shows a more complex distribution (Fig. 17B). The increased thickness of the Rupelton north of the Groß Schönebeck drillsite coincides partly with the assumed fractured area and may cause an additional damping of the seismic signal (Fig. 17C). In general, the seismic coverage decreases toward the surface, introducing some artefacts in the seismic volume and artificial discontinuities of the shallower seismic reflectors (Fig. 5).

Facies interpretation and model parameterization

The modelled facies and parameter distribution is aiming to reflect a realistic scenario of lateral and vertical structural and property distribution. The main restriction of the model is that the interpretation of the sedimentary facies of the Rotliegend needs to focus more or less on one location within the seismic volume (E GrSk 3/90 and Gt GrSk 4/05 boreholes) and that the volcanic sequence is not characterized by the wells completely.

The volcanic succession and a realistic property distribution is difficult to define. As the top of the sedimentary Carboniferous could not be resolved with certainty, neither from seismic or borehole data, this interpretation is lacking important input data. In addition, it seems more realistic, that several volcanoes are building up this sequence, resulting also in a more diverse flow and property distribution pattern of intercalated flows. Therefore, the presented interpretation and parameterization of the volcanic sequence represents a first-order approximation to enable further near-wellbore studies for site development, helping in identifying possible layouts and related risks of hydraulic stimulations and in estimating the geothermal potential of this sequence. As stress in the subsurface is expected to increase with depth, an upward fracture growth could be expected (see also Fig. 5 in Zimmermann et al. 2010). By stimulating the volcanic rock sequence, the fracture will tend to grow upward and may reach the overlying sedimentary Mirow Formation consisting of conglomerates and sandstones. Kushnir et al. (2018) report in a study related to the Upper Rhine Graben observations from outcrops showing that at the boundary to the crystalline basement low-permeable and high-strength sedimentary rocks were present. These rocks could also cap the crystalline basement hydraulically. In Groß Schönebeck, the petrophysical analysis of data from the E GrSk 3/90 borehole do indicate that the Mirow conglomerates above the volcanic succession exhibits a low matrix permeability. The hydraulic and most likely the mechanical properties of the sedimentary and volcanic rocks may be similar. The conglomerates, consisting of cemented volcanic rocks, show a similar porosity as the volcanic rocks. A weaker formation is expected in the overlying sandy deposits of the Dethlingen Formation, hosting the ERS. In the E GrSk 3/90 well, flow meter measurements from a production test performed after deepening of the well and prior to stimulation activities show some productive flow from an assumed natural fractured zone of conglomeratic and volcanic rocks but no flow from the Dethlingen Formation (Tischner et al. 2002). After a planned stimulation of the sandstones (isolated from the deeper conglomeratic and volcanic horizons by a sand pack), the productivity of the sandy interval was not improved (Legarth et al. 2005). Instead, the productivity of the deeper conglomeratic

horizon had increased, indicating that pre-existing fractures were most likely activated during stimulation. This is supported by temperature measurements showing that the fluid production temperatures are decreasing over time, documenting a hydraulic connection to the overlying (cooler) sandy unit (Tischner et al. 2002). However, the real propagation of induced fractures in Groß Schönebeck is not well constrained at all and may be triggered by the occurrence of natural (sub-seismic) fracture networks (for details and discussion see Blöcher et al. 2016). To design an adequate stimulation treatment of the volcanic Permo-Carboniferous rocks, the real thickness and composition (the lateral and vertical heterogeneity) and the structural and geomechanical properties of this unit (massive andesite vs. tuffitic layers) needs to be investigated in more detail. One option represents the deepening of the E GrSk 3/90 borehole by coring and logging until proven Carboniferous rocks were encountered.

The sedimentary Rotliegend could rely on a broader data set. Several boreholes nearby give evidence on the principal composition and the development of the sedimentary environment over time. The petrophysical well-log and core analysis reveals a profound facies-dependency of petrophysical properties. Focusing on the permeability characterization, the most robust correlation of porosity and permeability could be found in the ephemeral stream facies. This is in agreement with the mineralogical composition of the corresponding sandy reservoir: it represents a Quartz-dominated sandstone, and the permeability is not strongly affected by clay minerals (Holl 2002). The proportion of clay minerals and their textural properties plays a larger role for other sandy facies units, like the braided plains or sandy mudflat environment. The derived in-situ fluid permeabilities for unit 5 (ERS) ranges from less than 1 mD ($1\text{E}-15\text{ m}^2$) to more than 100 mD ($1\text{E}-13\text{ m}^2$), with an overall geometric mean of only some mD (Figs. 13, 14). The analysis of well tests at the Groß Schönebeck site (Blöcher et al. 2016) reports in the appendix transmissibility data of several hydraulic tests conducted. If we assume a reservoir thickness of the EBS of roughly 40 m at the wellsite, corresponding field permeabilities were in the same order, showing values of about 4 mD ($4\text{E}-15\text{ m}^2$).

Although the seismic data could not provide evidence for structural boundaries (block or fault compartments), the result of the facies and parameter modelling shows for unit 5 (EBS) slightly reduced reservoir properties along the Gt GrSk 4/05 borehole (Fig. 14). The range of variation is covered by the expected geological heterogeneity. However, the reconstruction of ancient fluvial system requires detailed information on its geometry in three dimensions. Former realizations did not consider the natural heterogeneity of the Permian reservoir but apply a layer-cake model of petrophysical properties, without consideration of lateral variability (Blöcher et al. 2016). The presented new model will be used for reservoir simulation, comparison, and future site development. First studies using a more realistic heterogeneous parameterization inspired by this study show that this may lead to a significant change in the long-term behaviour of the reservoir compared to a layer-cake model, allowing a much faster breakthrough along preferred flow paths, requiring a different well doublet layout. Moreover, the productivity of the system could be increased by an adapted exploitation concept, considering a more realistic property distribution (Bohnen 2020).

Further enhancement of the presented model parameterization could be achieved by inversion of the seismic data to better guide the distribution of petrophysical parameters. The inversion of the seismic volume may give some further insights on the property

distribution patterns and reservoir heterogeneity. Nevertheless, the inversion will also be limited by the scale and resolution of the geophysical (seismic) data and will not be able to resolve a detailed geological facies pattern and the accompanied petrophysical properties on a finer scale.

Conclusions

This work presents the results of an integrated study for reservoir characterization of a long-lasting deep geothermal research platform Groß Schönebeck by integrating available geophysical and geological data. Reservoir characterization by geological modeling is scale-sensitive. Integrating the available reconnaissance data with interpretations from the new 3D seismic survey and the DAS–VSP data and the borehole data allows constraining a much more realistic characterisation of the Rotliegend reservoir of the Groß Schönebeck research platform across different scales. Based on the structural data from 3D seismic and DAS–VSP geophysics as well as considering the geological (lithological and sedimentological) data from the boreholes, a new site and reservoir model was set up, following a facies-dependent distribution approach for its parameterization. In more detail, the new data allows a remapping of the thickness of the sandy EBS reservoir zone and adjacent horizons and their reservoir properties. The new 3D seismic data did not show any compartmentalization of the Rotliegend reservoir at the Groß Schönebeck site. Also the cores of the E GrSk 3/90 borehole do not show extensive fracturing. Nevertheless, joints and small faults of subtle and predominantly sub-seismic character may be present in the Rotliegend reservoir target. The case study Groß Schönebeck shows that the geothermal exploration of deep targets in the low-enthalpy setting should not rely solely on reconnaissance 2D-seismic lines, offset wells, and their (biased) structural interpretation. It is necessary to include 3D seismic analysis and its integrated interpretation to allow a more reliable site characterization and an adequate field development. Nevertheless, direct information from boreholes is thereby a prerequisite for this method. The thickness of the Permo-Carboniferous volcanic sequence, so far only indirectly deduced from geophysical borehole logging in one well, could not be clearly confirmed by the seismic data. To shed more light into the section below the sedimentary Rotliegend, a deepening of the E GrSk 3/90 borehole, preferably by coring, would allow to judge on the thickness and properties of the Permo-Carboniferous sequence. Further site development could rely on deviated wells in the Rotliegend and Permo-Carboniferous reservoirs with multi-stage stimulation to enhance the productivity of the reservoirs. The provided in-depth characterization is forming the basis for an ongoing evaluation of such and other exploitation strategies for the exploitation of deep geothermal reservoirs in the Northeast German Basin.

Acknowledgements

We thank Neptune Energy for support and the permission to use legacy exploration borehole and seismic data (profiles LEW) and the geological survey of Brandenburg (LBGR) for support in core sampling. We are grateful to Kristian Bär and an anonymous reviewer for their constructive comments that helped improving the quality of the manuscript.

Author contributions

BN, KB, and CK analysed and interpreted the geological and seismic data, BN performed the geological modelling and the facies and parameter parametrization of the reservoir targets, and was the major contributor writing the manuscript. All authors read and approved the final manuscript.

Funding

Open Access funding enabled and organized by Projekt DEAL. The seismic survey was funded by the German Federal Ministry for Economics within the project RissDom-A (Grant 0324065).

Availability of data and materials

The core and well-log data and applied analysis is provided in an accompanying data publication (Norden et al., 2022) at the GFZ repository that also includes the main geological horizons and a populated simulation grid of the parameterized reservoir model (<https://doi.org/10.5880/GFZ.4.8.2022.013>). The DAS–VSP data of Martuganova et al. (2022) is available also via the GFZ repository (<https://doi.org/10.5880/GFZ.4.8.2022.014>). The 3D seismic data sets used and/or analysed are available on request.

Declarations

Competing interests

The authors declare that they have no competing interests.

Received: 18 May 2022 Accepted: 18 December 2022

Published online: 06 January 2023

References

- Allen JRL. Physical processes of sedimentation. London: Allen and Unwin; 1970.
- Bauer K, Moeck I, Norden B, Schulze A, Weber M, Wirth H. Tomographic P-wave velocity and vertical velocity gradient structure across the geothermal site Groß Schönebeck (NE German Basin): relationship to lithology, salt tectonics, and thermal regime. *J Geophys Res*. 2010. <https://doi.org/10.1029/2009JB006895>.
- Bauer K, Norden B, Ivanova A, Stiller M, Krawczyk CM. Wavelet transform-based seismic facies classification and modeling: application to a geothermal target horizon in the NE German Basin. *Geophys Prospect*. 2020. <https://doi.org/10.1111/1365-2478.12853>.
- Belka Z, Devleeschouwer X, Narkiewicz M, Piecha M, Reijers TJA, Ribbert KH, Smith NJP. Devonian. In: Doornenbal JC, Stevenson AG, editors. *Petroleum geological atlas of the southern Permian Basin area*. Houten: EAGE Publications; 2010. p. 71–9.
- Benek R, Hoth P. Permokarbonische Vulkanite. In: Stackebrandt W, Manhenke V, editors. *Atlas zur Geologie von Brandenburg*. Kleinmachnow: Landesamt für Geowissenschaften und Rohstoffe Brandenburg (LGRB); 2004. p. 80.
- Benek R, Kramer W, McCann T, Scheck M, Negendank J, Korich D, Huebscher HD, Bayer U. Permo-carboniferous magmatism of the Northeast German Basin. *Tectonophysics*. 1996;266:379–404.
- Beutler G, Franz M, Keuper. In: Stackebrandt W, Franke D, editors. *Geologie von Brandenburg*. Stuttgart: Schweitzerbart; 2015. p. 194–216.
- Blöcher G, Reinsch T, Hennings J, Milsch H, Regensburg S, Kummerow J, Francke H, Kranz S, Saadat A, Zimmermann G, Huenges E. Hydraulic history and current state of the deep geothermal reservoir Groß Schönebeck. *Geothermics*. 2016. <https://doi.org/10.1016/j.geothermics.2015.07.008>.
- Blöcher G, Cacace M, Jacquey AB, Zang A, Heidbach O, Hofmann H, Kluge C, Zimmermann G. Evaluating micro-seismic events triggered by reservoir operations at the geothermal site of Groß Schönebeck (Germany). *Rock Mech Rock Eng*. 2018. <https://doi.org/10.1007/s00603-018-1521-2>.
- Bogie I, Mackenzie KM. The application of a volcanic facies model to an andesitic stratovolcano hosted geothermal system at Wayang Windu, Java, Indonesia. In: 20th New Zealand geothermal workshop. 1998. https://pangea.stanford.edu/ERE/db/IGStandard/record_detail.php?id=1827. Accessed 16 Feb 2022.
- Bohnen B. Investigation of the influence of heterogenous reservoir properties on the productivity and sustainability of the geothermal doublet system Groß Schönebeck. TU Berlin: master thesis; 2020.
- Breitkreuz C, Geißler M. Permokarbonische Vulkanite. In: Stackebrandt W, Franke D, editors. *Geologie von Brandenburg*. Stuttgart: Schweitzerbart; 2015. p. 110–6.
- Bridge JS, Mackey SD. A theoretical study of fluvial sandstone body dimensions. *Int Assoc Sedimentol Spec Publ*. 1993;15:213–36.
- Bridge JS, Tye RS. Interpreting the dimensions of ancient fluvial channel bars, channels, and channel belts from wireline-logs and cores. *Am Assoc Pet Geol Bull*. 2000;84(8):1205–28.
- Buness H, von Hartmann H, Rumpel H-M, Krawczyk CM, Schulz R. Fault imaging in sparsely sampled 3D seismic data using common-reflection-surface processing and attribute analysis—a study in the Upper Rhine Graben. *Geophys Prospect*. 2014. <https://doi.org/10.1111/1365-2478.12099>.
- Coates GR, Peveraro RCA, Hardwick A, Roberts D. The magnetic resonance imaging log characterized by comparison with petrophysical properties and laboratory core data. *SPE Annu Tech Conf Exhib*. 1991. <https://doi.org/10.2118/22723-MS>.
- DEKORP-BASIN Research Group. The deep crustal structure of the Northeast German basin: new DEKORP-BASIN'96 deep-profiling results. *Geology*. 1999. [https://doi.org/10.1130/0091-7613\(1999\)027%3c0055:DSCOTN%3e2.3.CO;2](https://doi.org/10.1130/0091-7613(1999)027%3c0055:DSCOTN%3e2.3.CO;2).
- Doornenbal H, Stevenson A. *Petroleum geological atlas of the southern Permian Basin area*. Houten: EAGE Publications BV; 2010.
- Emirov SN, Beybalaev VD, Gadzhiev GG, Ramazanova AE, Amirova AA, Aliverdiev AA. To the description of the temperature and pressure dependences of the thermal conductivity of sandstone and ceramics. *J Phys Conf Ser*. 2017;891:012335.
- Franke D. Devon. In: Stackebrandt W, Franke D, editors. *Geologie von Brandenburg*. Stuttgart: Schweitzerbart; 2015a. p. 73–83.

- Franke D. Flyschoides Karbon. In: Stackebrandt W, Franke D, editors. *Geologie von Brandenburg*. Stuttgart: Schweitzerbart; 2015b. p. 83–95.
- Fuchs S, Förster A. Well-log based prediction of thermal conductivity of sedimentary successions: a case study from the North German Basin. *Geophys J Int*. 2014. <https://doi.org/10.1093/gji/ggt382>.
- Fuchs S, Balling N, Förster A. Calculation of thermal conductivity, thermal diffusivity and specific heat capacity of sedimentary rocks using petrophysical well logs. *Geophys J Int*. 2015. <https://doi.org/10.1093/gji/ggv403>.
- García A, Contreras E, Viggiano JC. Establishment of an empirical correlation for estimating the thermal conductivity of igneous rocks. *Int J Thermophys*. 1989. <https://doi.org/10.1007/BF00503174>.
- Gardner GHF, Gardner LW, Gregory AR. Formation velocity and density—the diagnostic basics for stratigraphic traps. *Geophysics*. 1974. <https://doi.org/10.1190/1.1440465>.
- Gast RE. 2.6 Sequenzstratigraphie. In: Plein E, editor. *Stratigraphie von Deutschland I—Norddeutsches Rotliegendbecken, Rotliegend-Monographie Teil II*. Frankfurt: Courier Forschungsinstitut Senckenberg; 1995. p. 47–54.
- Gast RE, Gebhardt U. 4.4 Elbe-Subgruppe. In: Plein E, editor. *Stratigraphie von Deutschland I—Norddeutsches Rotliegendbecken, Rotliegend-Monographie Teil II*. Frankfurt: Courier Forschungsinstitut Senckenberg; 1995. p. 121–35.
- Gast RE, Pasternak M, Piske J, Rasch H-J. Das Rotliegend im nordostdeutschen Raum: Regionale Übersicht, Stratigraphie, Fazies und Diagenese. *Geol Jahrb Reihe A*. 1998;149:59–79.
- Gast RE, Duser M, Breikreuz C, Gaupp R, Schneider JW, Stemmerik L, Geluk MC, Geisler M, Kiersnowski H, Glennie KW, Kabel S, Jones NS. Rotliegend. In: Doornenbal JC, Stevenson AG, editors. *Petroleum Geological Atlas of the Southern Permian Basin area*. Houten: EAGE Publications; 2010. p. 101–21.
- Gebhardt U, Schneider J, Hoffmann N. Modelle zur Stratigraphie und Beckenentwicklung im Rotliegenden der Norddeutschen Senke. *Geol Jahrb Reihe a*. 1991;127:405–27.
- Geißler M, Breikreuz C, Kiersnowski H. Late Paleozoic volcanism in the central part of the Southern Permian Basin (NE Germany, W Poland): facies distribution and volcano-topographic hiatus. *Int J Earth Sci*. 2008;97(5):973–89.
- Gibling MR. Width and thickness of fluvial channel bodies and valley fills in the geological record: a literature compilation and classification. *J Sediment Res*. 2006;76(5):731–70.
- Hamann M, Kuhlee, Schulz W, Priebe. Geologisch-technisch-oekonomischer Abschlussbericht der Bohrung E Gross Schönebeck 3/90, Erdöl-Erdgas Grimmen GmbH, Hauptabteilung Geologie, Grimmen, 24.5.1991, 66 pages and 11 enclosures. **(in German)**.
- Hardt J, Norden B, Bauer K, Toelle O, Krumbach J. Surface cracks—geomorphological indicators for late Quaternary halotectonic movements in northern Germany. *Earth Surf Process Landf*. 2021. <https://doi.org/10.1002/esp.5226>.
- Heap MJ, Kushnir ARL, Vasseur J, Wadsworth FB, Harlé P, Baud P, Kennedy BM, Troll VR, Deegan FM. The thermal properties of porous andesite. *J Volcanol Geoth Res*. 2020. <https://doi.org/10.1016/j.jvolgeores.2020.106901>.
- Henninges J, Martuganova E, Stiller M, Norden B, Krawczyk CM. Wireline distributed acoustic sensing allows 4.2 km-deep vertical seismic profiling of the Rotliegend 150°C-geothermal reservoir in the North German Basin. 2021. *Solid Earth*. <https://doi.org/10.5194/se-12-521-2021>.
- Holl HG. Clay minerals and cementation of clastic sediments of the Havel and Elbe Subgroups (Late Rotliegend) derived from cores of the borehole Groß Schönebeck 3/90. In: Huenges E, Hurter S, editors. *In-situ Geothermielabor Groß Schönebeck 2000/2001*. Scientific Technical Report STR02/14. 2002. <https://doi.org/10.23689/fidgeo-522>.
- Holl HG, Moeck I, Schandlmeier H. Characterization of the tectono-sedimentary evolution of a geothermal reservoir—implications for exploitation (Southern Permian Basin, NE Germany), (Proceedings), World Geothermal Congress (Antalya Turkey). 2005. <https://www.geothermal-energy.org/pdf/IGAStandard/WGC/2005/0614.pdf>. Accessed 16 Feb 2022.
- Hoth K, Huebscher H-D. Vulkanite der DDR (Lithogenetische und paläogeomorphologische Charakteristik sowie Rayonierung der Autoneffusiva im Norden der DDR), VEB Geologische Forschung und Erkundung Freiberg, 1986. Map 1:500.000. **(in German)**.
- Hoth K, Ruspült J, Zagora K, Beer H, Hartmann O. Die tiefen Bohrungen im Zentralabschnitt der Mitteleuropäischen Senke - Dokumentation für den Zeitabschnitt 1962–1990, vol. 2. Berlin: Schriftenr geol Wiss; 1993. p. 145.
- Huebscher H-D. Zur epigenetischen Metasomatose in den permosilesischen basaltischen Mg-Andesiten von Ost-Brandenburg. *Deutschland Terra Nostra*. 1995;7:63–6.
- Huenges E. Einleitung. In: Huenges E, Hurter S, editors. *In-situ Geothermielabor Groß Schönebeck 2000/2001*. Scientific Technical Report STR02/14. 2002. <https://doi.org/10.23689/fidgeo-522>.
- Huenges E, Hurter S, editors. *In-situ Geothermielabor Groß Schönebeck 2000/2001*. Scientific Technical Report STR02/14. 2002. <https://doi.org/10.23689/fidgeo-522>.
- Huenges E, Winter H. Experimente zur Produktivitätssteigerung in der Geothermie-Forschungsbohrung Groß Schönebeck 3/90, Scientific Technical Report, GeoForschungsZentrum Potsdam, STR 04/16; 2004. p.76–92. <https://doi.org/10.48440/gfz.b103-04164>. **(in German)**.
- Jakubowicz H. Wave equation prediction and removal of interbed multiples. In: 68th annual international meeting, SEG, expanded abstracts. 1998. <https://doi.org/10.1190/1.1820204>.
- Juhász I. Conversion of routine air permeability data into stressed brine-permeability data. In: SPWLA tenth European formation evaluation symposium, Aberdeen, UK. 1986. p. 15.
- Kana JD, Djongyong N, Raïdandi D, Nouck PN, Dadjé A. A review of geophysical methods for geothermal exploration. *Renew Sust Energy Rev*. 2015. <https://doi.org/10.1016/j.rser.2014.12.026>.
- Klinkenberg LJ. The permeability of porous media to liquids and gases. *Drill Prod Pract*. 1941;2:200–13.
- Kombbrink H, Besly BM, Collinson JD, Den Hartog Jager DG, Drozdowski G, Duser M, Hoth P, Pagnier HJM, Stemmerik L, Waksmundzka MI, Wrede V. Carboniferous. In: Doornenbal JC, Stevenson AG, editors. *Petroleum geological atlas of the southern Permian Basin area*. Houten: EAGE Publications; 2010. p. 81–99.
- König H, Meyer W. Ergebnisbericht Finow 2.1/Liebenwalde 2.1, VEB Kombinat Erdöl-Erdgas Gommern, 15.11.1988, p.35. **(in German)**.
- Kopp J, Hoffmann N, Lindert W, Franke D. Präpermischer Untergrund - Tektonostratigraphie und Bruchstörungen. In: Stackebrandt W, Manhenke V, editors. *Atlas zur Geologie von Brandenburg*. Kleinmachnow: Landesamt für Geowissenschaften und Rohstoffe Brandenburg (LGRB); 2004. p. 80.

- Kossow D, Krawczyk CM. Structure and quantification of factors controlling the evolution of the inverted NE German Basin. *Mar Pet Geol*. 2002;19(5):601–18.
- Kossow D, Krawczyk CM, McCann T, Strecker M, Negendank JFW. Style and evolution of salt pillows and related structures in the northern part of the Northeast German Basin. *Int J Earth Sci*. 2000;89(3):652–64.
- Krawczyk CM, Henk A, Tanner DC, Trappe H, Ziesch J, Beilecke T, Aruffo CM, Weber B, Lippmann A, Görke U-J, Bilke L, Kolditz O. Seismic and sub-seismic deformation prediction in the context of geological carbon trapping and storage. *Adv Technol Earth Sci*. 2015. https://doi.org/10.1007/978-3-319-13930-2_5.
- Krawczyk CM, Stiller M, Bauer K, Norden B, Hennings J, Ivanova A, Huenges E. 3-D seismic exploration across the deep geothermal research platform Groß Schönebeck north of Berlin/Germany. *Geotherm Energy*. 2019. <https://doi.org/10.1186/s40517-019-0131-x>.
- Kushnir ARL, Heap MJ, Baud P, Gilg A, Reuschlé T, Lerouge C, Dezayes C, Düringer P. Characterizing the physical properties of rocks from the Paleozoic to Permo-Triassic transition in the Upper Rhine Graben. *Geotherm Energy*. 2018. <https://doi.org/10.1186/s40517-018-0103-6>.
- Kwiatk G, Bohnhoff M, Dresen G, Schulze A, Schulte T, Zimmermann G, Huenges E. Microseismicity induced during fluid-injection: a case study from the geothermal site at Groß Schönebeck, North German Basin. *Acta Geophys*. 2010. <https://doi.org/10.2478/s11600-010-0032-7>.
- Lange G, Söllig A, Tessin R, Berlin ZGL. Isobathen der Zechsteinbasis 1:500.000. VEB Kartographischer Dienst Potsdam, Zentrales Geologisches Institut, Berlin; 1981.
- Le Maitre RW. *Igneous rocks: a classification and glossary of terms*. Cambridge: Cambridge University Press; 2002. p. 252.
- Leclair SF, Bridge JS. Quantitative interpretation of sedimentary structures formed by river dunes. *J Sediment Res*. 2001;71(5):713–6.
- Legarth B, Huenges E, Zimmermann G. Hydraulic fracturing in a sedimentary geothermal reservoir: results and implications. *Int J Rock Mech Min Sci*. 2005. <https://doi.org/10.1016/j.jrmms.2005.05.014>.
- Lindert W, Warncke D, Stumm M. Probleme der lithostratigraphischen Korrelation des Oberrotliegenden (Saxon) im Norden der DDR. *Z Angew Geol*. 1990;36(10):368–75.
- Lokhorst A. *NW European gas atlas*. Haarlem: Nederlands Inst. voor Toegepaste Geowetenschappen TNO. 1 CD-ROM; 1998.
- Lotz B. Neubewertung des rezenten Wärmestroms im Nordostdeutschen Becken. Potsdam: Scientific Technical Report 04/04. 2004. <http://d-nb.info/971558531/34>. Accessed 16 Feb 2022.
- Mann J, Jäger R, Müller T, Höcht G, Hubral P. Common-reflection-surface stack—a real data example. *J Appl Geophys*. 1999. [https://doi.org/10.1016/S0926-9851\(99\)00042-7](https://doi.org/10.1016/S0926-9851(99)00042-7).
- Martuganova E, Stiller M, Norden B, Hennings J, Krawczyk CM. 3D deep geothermal reservoir imaging with wireline distributed acoustic sensing in two boreholes. 2022. *Solid Earth*. <https://doi.org/10.5194/se-2021-138>.
- McCann T. Sandstone composition and provenance of the Rotliegend of the NE German Basin. *Sediment Geol*. 1998;116(3–4):177–98.
- McGuire JJ, Lohman RB, Catchings RD, Rymer MJ, Goldman MR. Relationships among seismic velocity, metamorphism, and seismic and aseismic fault slip in the Salton Sea Geothermal Field region. *J Geophys Res Solid Earth*. 2015. <https://doi.org/10.1002/2014JB011579>.
- Mendrinis D, Chorapanitis I, Polyzou O, Karytsas C. Exploring for geothermal resources in Greece. *Geothermics*. 2010. <https://doi.org/10.1016/j.geothermics.2009.11.002>.
- Moekel I, Schandelmeier H, Holl HG. The stress regime in a Rotliegend reservoir of the Northeast German Basin. *Int J Earth Sci*. 2009. <https://doi.org/10.1007/s00531-008-0316-1>.
- Norden B, Bauer K, Krawczyk CM. Input and resulting structural and parameterized subsurface data for a geological model of the geothermal research platform Groß Schönebeck (North German Basin). *GFZ Data Services*. 2022. <https://doi.org/10.5880/GFZ.4.8.2022.013>.
- Peryt TM, Geluk MC, Mathiesen A, Paul J, Smith K. Zechstein. In: Doornenbal JC, Stevenson AG, editors. *Petroleum geological atlas of the southern Permian Basin area*. Houten: EAGE Publications; 2010. p. 123–47.
- Plein E. *Stratigraphie von Deutschland I - Norddeutsches Rotliegendebcken, Rotliegend-Monographie Teil II*. Frankfurt: Courier Forschungsinstitut Senckenberg; 1995.
- Pussak M, Bauer K, Stiller M, Bujakowski W. Improved 3D seismic attribute mapping by CRS stacking instead of NMO stacking: application to a geothermal reservoir in the Polish basin. *J Appl Geophys*. 2014. <https://doi.org/10.1016/j.jappgeo.2014.01.020>.
- Regenspurg S, Feldbusch E, Norden B, Tichomirowa M. Fluid-rock interactions in a geothermal Rotliegend/Permo-Carboniferous reservoir (North German Basin). *Appl Geochem*. 2016. <https://doi.org/10.1016/j.apgeochem.2016.03.010>.
- Reinhardt H-G. Structure of Northeast Germany: regional depth and thickness maps of Permian to Tertiary intervals compiled from seismic reflection data. *Spec Publ Eur Assoc Pet Geosci*. 1993;3:155–65.
- Ricard LP, Huddleston-Holmes CR, Pujol M. Reservoir and production engineering challenges for geothermal systems hosted in Australian Sedimentary Basins. *Soc Pet Eng*. 2016. <https://doi.org/10.2118/182343-MS>.
- Rider M. The geological interpretation of well logs. *Caithness: Whittles Publ*; 2000. p. 280.
- Rieke H. *Sedimentologie, Faziesarchitektur und Faziesentwicklung des kontinentalen Rotliegenden im Norddeutschen Becken (NEDB)*. Potsdam: Scientific Technical Report STR 01/14. 2001. <https://doi.org/10.48440/GFZ.b103-010029>.
- Rieke H, Kossow D, McCann T, Krawczyk CM. Tectono-sedimentary evolution of the northernmost margin of the NE German Basin between uppermost Carboniferous and Late Permian (Rotliegend). *Geol J*. 2001;36(1):19–37.
- Rieke H, McCann T, Krawczyk CM, Negendank JFW. Evaluation of controlling factors on facies distribution and evolution in an arid continental environment: an example from the Rotliegend of the NE German Basin. In: McCann T, Sainot A, editors. *Tracing tectonic deformation using the sedimentary record*. *Geol Soc Spec Publ*. 2003;208:71–94.
- Rockel W, Hurter S. Tiefe Altbohrungen als Beitrag zur Nutzbarmachung klüftig-poröser Speichergesteine (geologische Grundlagen): Groß Schönebeck. *Scientific Technical Report STR00/23*. 2000. p. 29–50. <https://doi.org/10.48440/gfz.b103-00236>. (in German).

- Scheck M, Bayer U. Evolution of the Northeast German Basin—inferences from a 3D structural model and subsidence analysis. *Tectonophysics*. 1999;313(1–2):145–69.
- Scheck M, Bayer U, Lewerenz B. Salt movements in the Northeast German Basin and its relation to major post-Permian tectonic phases—results from 3D structural modelling, backstripping and reflection seismic data. *Tectonophysics*. 2003;361(3–4):277–99.
- Scheck-Wenderoth M, Maystrenko Y, Hübscher C, Hansen M, Mazur S. Dynamics of salt basins. In: Littke R, Bayer U, Gajewski D, Nelskamp S, editors. *Dynamics of complex sedimentary basins. The Central European basin system*. Berlin: Springer; 2008. p. 307–22.
- Sekiguchi KA. A method for determining terrestrial heat flow in oil basinal areas. *Tectonophysics*. 1984;103:67–79.
- Siler DL, Faulds JE, Mayhew B, McNamara DD. Analysis of the favorability for geothermal fluid flow in 3D: Astor Pass geothermal prospect, Great Basin, northwestern Nevada, USA. *Geotherm*. 2016. <https://doi.org/10.1016/j.geothermics.2015.11.002>.
- Siratovich PA, Heap MJ, Villeneuve MC, Cole JW, Reuschlé T. Physical property relationships of the Rotokawa Andesite, a significant geothermal reservoir rock in the Taupo Volcanic Zone, New Zealand. *Geotherm Energy*. 2014. <https://doi.org/10.1186/s40517-014-0010-4>.
- Somerton WH. *Thermal properties and temperature-related behavior of rock/fluid systems*. Amsterdam: Elsevier Science Publishers; 1992.
- Stackebrandt W, Manhenke V. *Atlas zur Geologie von Brandenburg*. Cottbus: Landesamt für Bergbau, Geologie und Rohstoffe; 2010.
- Stackebrandt W, Röhling HG. Trias – Geologischer Rahmen. In: Stackebrandt W, Franke D, editors. *Geologie von Brandenburg*. Stuttgart: Schweitzerbart; 2015. p. 144–7.
- Strozyk F, Van Gent H, Urai JL, Kukla PA. 3D seismic study of complex intra-salt deformation: an example from the Upper Permian Zechstein 3 stringer, western Dutch offshore. *Geol Soc Spec Publ*. 2012. <https://doi.org/10.1144/SP363.23>.
- Strozyk F, Reuning L, Scheck-Wenderoth M, Tanner DC. Chapter 10—The tectonic history of the Zechstein Basin in the Netherlands and Germany. In: Soto JI, Flinch JF, Tari G, editors. *Permo-triassic salt provinces of Europe, North Africa and the atlantic margins*. Amsterdam: Elsevier; 2017. p. 221–41.
- Tischner T, Thorenz C, Jung R, Kessels W. Results from a production test: hydraulics. In: Huenges E, Hurter S, editors. *In-situ Geothermielabor Groß Schönebeck 2000/2001*. Scientific Technical Report STR02/14. 2002. <https://doi.org/10.23689/idgeo-522>.
- Trautwein U, Huenges E. Poroelastic behaviour of physical properties in Rotliegend Sandstones under uniaxial strain, Internat. *J Rock Mech Min Sci*. 2005;42(7–8):924–32.
- Trautwein U. *Poroelastische Verformung und petrophysikalische Eigenschaften von Rotliegend Sandsteinen*. Berlin: Dissertation TU Berlin. 2005. https://depositonce.tu-berlin.de/bitstream/11303/1537/1/Dokument_47.pdf. Accessed 16 Feb 2022.
- van Wees J-D, Stephenson RA, Ziegler PA, Bayer U, McCann T, Dadlez R, Gaupp R, Narkiewicz M, Bitzer F, Scheck M. On the origin of the Southern Permian Basin, Central Europe. *Mar Pet Geol*. 2000;17:43–59.
- von Hartmann H, Beilecke T, Bunes H, Musmann P, Schulz R. Seismische exploration für tiefe Geothermie. *Geol Jahrb*. 2015;B104:1–271.
- Waples DW, Waples JS. A review and evaluation of specific heat capacities of rocks, minerals, and subsurface fluids. Part 1: minerals and nonporous rocks. *Nat Resour Res*. 2004. <https://doi.org/10.1023/B:NARR.0000032647.41046.e7>.
- Wyllie MRJ, Gregory AR, Gardner LW. Elastic wave velocities in heterogeneous and porous media. *Geophysics*. 1956;21(1):41–70.
- Zhang X, Hu Q. Development of geothermal resources in China: a review. *J Earth Sci*. 2018. <https://doi.org/10.1007/s12583-018-0838-9>.
- Zhang Y, Krause M, Mutti M. The formation and structure evolution of Zechstein (Upper Permian) salt in Northeast German basin: a review. *Open J Geol*. 2013. <https://doi.org/10.4236/ojg.2013.38047>.
- Ziegler PA. *Geological atlas of western and Central Europe*. 2nd ed. The Hague: Shell; 1990.
- Zimmermann G, Moeck I, Blöcher G. Cyclic waterfrac stimulation to develop an enhanced geothermal system (EGS)—conceptual design and experimental results. *Geothermics*. 2010. <https://doi.org/10.1016/j.geothermics.2009.10.003>.

Publisher's Note

Springer Nature remains neutral with regard to jurisdictional claims in published maps and institutional affiliations.

Submit your manuscript to a SpringerOpen[®] journal and benefit from:

- Convenient online submission
- Rigorous peer review
- Open access: articles freely available online
- High visibility within the field
- Retaining the copyright to your article

Submit your next manuscript at ► [springeropen.com](https://www.springeropen.com)